

Radio Frequency Measurement and Modeling of Miniaturized Components for High-Speed Applications



Deutscher Akademischer Austauschdienst
German Academic Exchange Service

DAAD Project No. 57531629

TUHH

Hamburg University of Technology

Institut für Theoretische Elektrotechnik

Work Report

by

Dr. Yifan Qian

20.12.2022

This is the work report of project No. 57531629 supported by DAAD (Deutscher Akademischer Austauschdienst) and CSC (China Scholarship Council), written by Dr. Yifan Qian, supervised by Prof. Schuster and Dr. Yang, lasts from July 10th, 2021 to December 31st 2022.

Outline

1 Original Project Proposal.....	4
1.1 Current State of Research.....	4
1.2 Preliminary Work and Research Objectives.....	4
1.3 Research Strategies.....	6
2 Simulation & Measurement Training.....	7
2.1 Full-Wave Simulations	7
2.1.1 Microstrip Line	7
2.1.2 Microstrip Antenna	10
2.1.3 Bonding Wires.....	11
2.2 Calculation of Complex Permittivity.....	12
2.3 Measurement of Coaxial Cables	15
2.4 Summary.....	18
3 TRL Calibration Theory and Practice.....	20
3.1 Derivation	21
3.2 Implementation	26
3.2.1 Implementation of Section 2.1.1.....	26
3.2.2 Implementation without SMA Connector	27
3.2.3 Three-Dimension Model Optimization	31
3.3 Measurement.....	36
3.3.1 Comparison	36
3.3.2 Optimization.....	38
3.4 Verification	43
3.5 Summary.....	44
4 De-embedding of 3D Element Package	46
4.1 Simulation Verification	47
4.2 Experiment Verification.....	48
4.3 Summary.....	51
5 Fabrication Overview	52
5.1 Fabrication Method	52
5.2 Fabricated Calibration Structures	54
6. Conclusions and Recommendations.....	58
7 References.....	59

1 Original Project Proposal

In order to achieve balance between complexity, efficiency, and accuracy of miniaturized components, this research project aimed at developing parameterized and scalable model generation. The key research topics are focusing at parasitic effects analysis, de-embedding processing with TRL (Thru-Reflect-Line) calibration techniques and model synthesis.

1.1 Current State of Research

With increasing development of high-speed and high-integration electric and electronic systems, miniaturized components, for example, surface mounted device (SMD) capacitors, diodes, transistors and monolithic microwave integrated circuit (MMIC), are widely used in distributed radio frequency (RF) designs. As a result, accurate modeling of the impedance characteristic for miniaturized components becomes a concern in final designs. First, the size of miniaturized components is in the millimeter and submillimeter range that brings difficulty to high frequency measurements and an additional fixture is needed. Second, component packaging produces complex parasitics in RF designs which should be precisely investigated to avoid significant performance degradation. Third, customized applications and simulation tools request different variations of using miniaturized components, such as changing substrate materials of printed circuit boards (PCB), layout sizes, choosing planar or full-wave interfaces, resulting in an issue of modeling scalability.

Since the 1960s, Scattering parameters (S-parameters) and vector network analyzer have enabled dramatic advances in RF measurement and modeling techniques. Among them, a calibration and de-embedding technique, so called Thru-Reflect-Line (TRL)[1], was successfully applied for measuring the S-parameters of miniaturized components and was adopted by RF discrete manufactures for decades up to nowadays[2]. The de-embedded S-parameters can be transformed into a netlist, an equivalent circuit including R, L, C and control sources, for general simulation with sophisticated techniques[3][4]. When considering field interactions with components, such as reconfigurable antennas, the de-embedded S-parameters and equivalent circuits might be inadequate because of an incomplete 3D full-wave simulation model of components and inevitable parasitic effects from local grounds, soldering pads[5]. Also the final application environment might be inconsistent with the one of measurement[6]. In such circumstances, full-wave electromagnetic (EM) model of RF components, including packaging, geometry, material composition, is proposed for accurate characterization of field-circuit couplings in application environment and numerical calibration techniques are used for removing parasitic effects[7][8][9].

The full-wave EM model has advantages of improved accuracy but shows high complexity and low efficiency by integrating manufacturing designs into simulation. Consequently, the computation cost and stability of the whole design become an issue when applying over discretized meshes of a component at high frequencies. Considering inside fields of a component are not of interests for most RF designs, such as signal/power integrity (SI/PI), Electrostatic Discharge (ESD) protection and electrically reconfiguration antennas, a parameterized, scalable model is proposed here with emphasis on the numerical characterization of miniaturized components with model-to-hardware correlations. In special, the redundant computation of component in full-wave simulations will be optimized with considerable reductions and parasitic effects from different stages of manufacturing, testing and simulation will be separated using measurement and numerical de-embedding techniques for enhancing modeling scalability.

1.2 Preliminary Work and Research Objectives

During the PhD study, the applicant has engaged numerical simulations with respect to transient investigations of fields-circuit problems[10]. The fundamental tasks of this project, such as full-circuit co-simulations, lumped port modeling, are consistent with the applicant's previous studies. The extended work with preliminary investigations, for example, parasitic effects analysis, de-embedding processing, are well selected for enhancing the applicant's professional knowledge and programming skills.

The host research group, the Institut für Theoretische Elektrotechnik (Institute of Electromagnetic Theory) at Hamburg University of Technology (TUHH) headed by Prof. Christian Schuster, has great advantages in the modeling and simulation of field-circuit coupling problems and extensive experience in hosting academic guests, including joint BS/MS/PhD students, PostDocs, Alexander-von-Humboldt (AvH) fellows. The host can offer high-performance computational resources and measurement equipments to support this project[11][12]. Also high-quality academic training and guidance are provided.

Table 1 Research Schedule

Date	Schedule
Jul. 2021 ~ Oct. 2021	Software and coding training. Several kinds of models such as microstrip line, microstrip antenna, patch R/L/C elements and wires are utilized in the simulation training. Reasonable results have to be achieved, calibration code is completed and verified by simulation data.
Oct. 2021 ~ Jan. 2022	Hardware and fabrication training. The calibration fixture is fabricated in the laboratory and measured by the Vector Network Analyze machine. The connector from coaxial to PCB and calibration code are implemented from 10MHz ~ 6GHz.
Jan. 2022 ~ Apr. 2022	Fixture optimization. Calibration fixture is updated by optimizing the transmission quality of launch. More reliable calibration result is obtained from 10MHz ~ 18GHz.
Apr. 2022 ~ Aug. 2022	Measurement verification and the manuscript of IEEE Magazine. Real element is implemented on the fixture and the calibrated result is obtained. The comparison between simulation and measurement is analyzed. The manuscript of IEEE magazine is completed.
Aug. 2022 ~ Dec. 2022	Implementation and de-embedding for higher frequency. Based on the TRL calibration data, a de-embedding equation is implemented for further element package de-embedding. The SMA connector and transmission line are all improved for higher frequency fixture implementation from 10MHz ~ 40GHz. This research project can be possibly extended for further achievement.

The research objectives of this project are mainly shown as follows:

- (1) Parasitic effects analysis: It is well known that manufacturing and testing procedures of miniaturized components introduces physical parasitic effects for modeling, such as bonding wires inside a package, solder pads on PCBs, testing cables and adaptors. However, an improper using of lumped ports, i.e. numerical interface between electric small elements to distributed EM structures, also brings virtual parasitic effects into simulation. For example, the lumped assumption of small size gap surface with negligible phase variations might be invalid for miniaturized components operating at tens of GHz. Therefore, a comprehensive analysis of parasitic effects is conducted.
- (2) De-embedding processing: Using sophisticated calibration techniques, TRL for example, the reference plane of measurements can be shifted to the adjacent area of the device under test. But the local ground and the pads effects are not removed in the final measurement de-embedding results. Therefore, a full-wave simulation assisted numerical de-embedding processing is proposed. Besides, when the frequency

is up to tens of GHz, the 8-term TRL error model should be carefully adapted because of increased radiation emissions and couplings of different portions of the testing fixture.

(3) Model synthesis: The scalability of a model states for the applicability of using one model for various applications with little or no modifications. As explained, the lumped port setting in full-wave modeling results in parasitic effects (discontinuities from pads to port, ground couplings). Therefore, the port modeling is optimized from multiple application environments and the corresponding parasitic separation procedure and the performance profiling is carried out.

1.3 Research Strategies

The duration of the project is about one year and a half (July 2021 ~ December 2022). During this period, we focused on full-wave simulations, computer programming, high frequency measurements and experimental validations, successively. The entire research content closely fits the original research proposal, and there are also some extended research on some valuable points that can be investigated deeper. Specifically, the time schedule is shown in Table 1.

2 Simulation & Measurement Training

The first part was to complete the software and hardware training (2 months), which was also a meaningful way to start the research project. Although the applicant had some experience in high-frequency simulation for 3D models, it was still necessary to take some relative 3D simulation training of this project. At the same time, it also helped strengthen knowledge about high frequency electromagnetics. Two popular commercial electromagnetic simulation software are used for simulation.

2.1 Full-Wave Simulations

Accurate modeling and simulation of miniaturized components are difficult. To start the research project in a responsible way, while consolidating the theoretical foundation, simulation must be taken to deepen the understanding of the electromagnetic effects of micro devices instead of experiment. Achieving accurate simulation is the first step. At this stage, two popular commercial electromagnetic simulation software are used to simulate the same model, and whether the simulation results are consistent is a criterion to judge whether the simulation is effective.

At the beginning of this project, some initial preparations have to be completed. Various algorithms of electromagnetic calculation, especially the transmission line method should be studied[13], operation of two commercial simulation software should be reviewed[14][15], the references of the research proposal should be read carefully again as well as the books recommended by the supervisor[16]. Information of two topics 'Linear Algebra' and 'Microelectronic Element' from website, books, colleagues, memories be should pay attention to. Literatures about EMC, MTT, CPMT transactions should be read and the scholarship holder should also pay attention to the key words 'de-embedding', 'parasitics', 'parasitic elements' and find out the research progress of the frontier in the world. At the same time, applicant has to complete a good monthly report every three months and a short summary after every weekly meeting. That is important to the research project as well as the improvement of scientific research ability for the scholarship holder himself.

To successfully complete the TRL (thru-reflect-line) calibration, accurate simulation is needed. To make sure the simulation is right, not only the transmission line but also other typical models such as microstrip antenna, will be simulated under a certain frequency range and their both results in FIT method (Finite Integration Technique) and FEM method (Finite Elements Method) will be compared to guarantee the accuracy. The simulation of transmission line is presented in section 2.1.1, the simulation of microstrip antenna is presented in section 2.1.2.

2.1.1 Microstrip Line

The transmission line is a typical structure for TRL calibration, so the accuracy of simulation on a transmission line is important. In this report, all the characteristic impedance of microstrip line is 50Ohm. In this section, two similar results of simulations for a transmission line structure by two commercial tools are regarded as the simulation target. The schematic of transmission line cross section is show in Fig. 1. The height of the substrate is $h=20\text{mil}=0.508\text{mm}$, the width of line is $w=1.07\text{mm}$, the height of ground is $35\mu\text{m}$, the whole length of substrate is $L=50\text{mm}$, the whole width of substrate is $W=30\text{mm}$, the material of line and ground is 'copper', the material of substrate is RO4350 (lossy free), the permittivity is $\epsilon_{\text{RO4350}}=3.66$. The frequency range is from 0GHz to 5GHz.

Accuracy simulation of such transmission line is a prerequisite of TRL calibration. In order to ensure the accuracy of the simulation, two simulation software are utilized to simulate it, and ensure that in the both ways can almost the same results been obtained when the structural parameters, materials, excitation types, and frequency ranges are the same. The object to be compared is the S-parameter, and in order to ensure the consistency of the characteristic impedance, the touchstone files of the two software's results will be imported into the third software for verification.

All the excitations are set as waveguide ports, the ports directly attach the copper ground, the width and height of ports is $w_{\text{ports}}=w+h*14=1.07+0.508*14=8.182\text{mm}$, $h_{\text{ports}}=0.035+h*8=4.099\text{mm}$. In Fig. 2(a), the

boundaries is set as an example from the website[17].

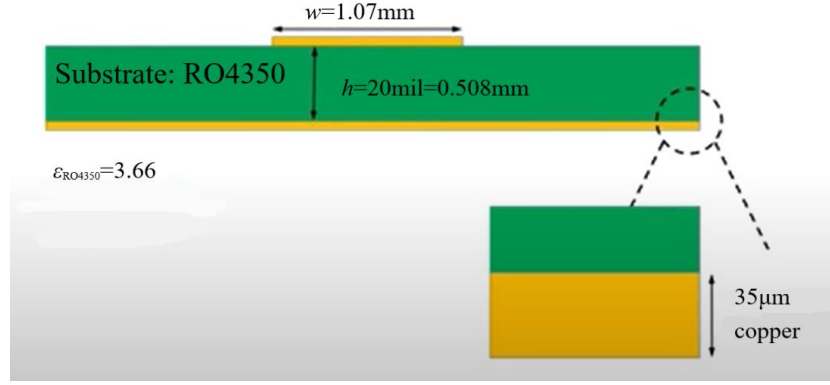


Fig. 1 Schematic of transmission line cross section

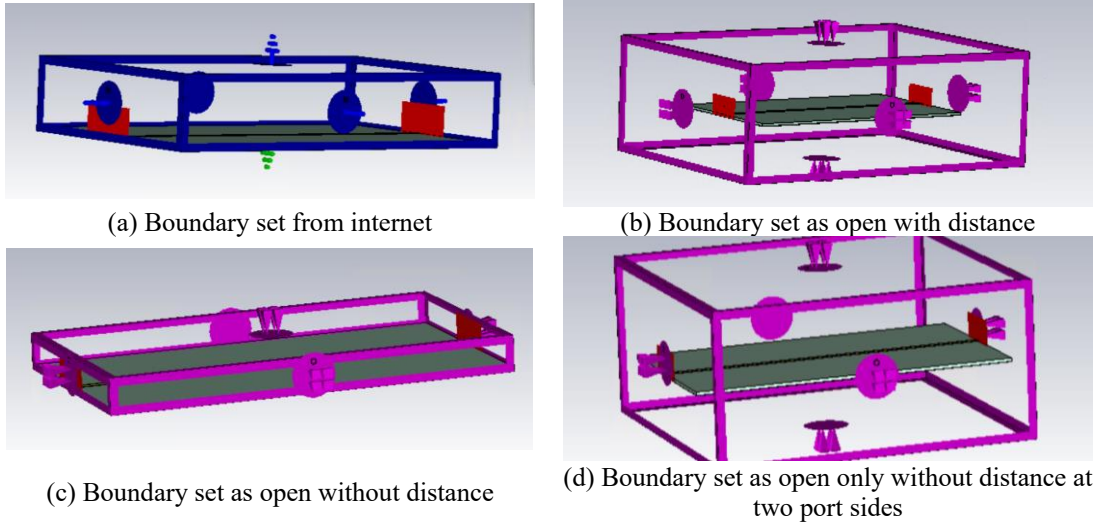


Fig. 2 Four Schematic of setting in a commercial software

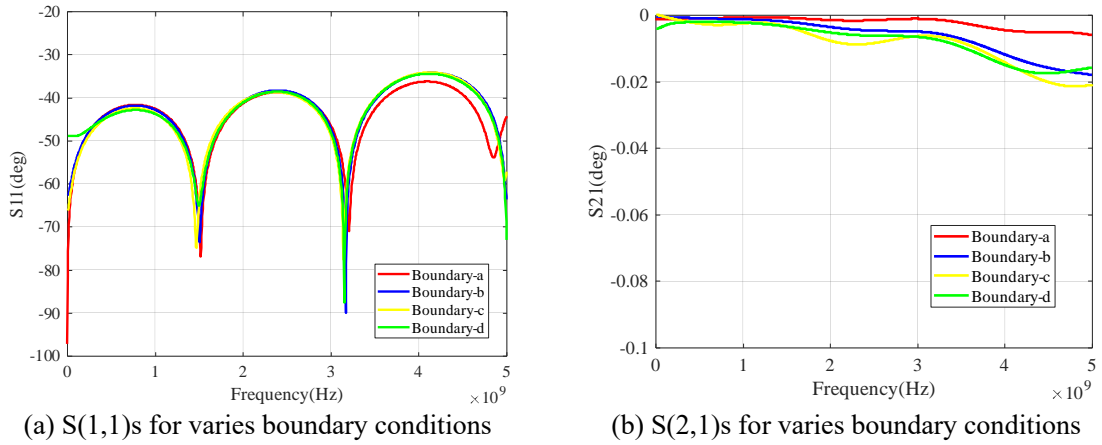


Fig. 3 Results of the four S-parameters in FIT (red for (a), blue for (b), yellow for (c), green for (d))

There is 5mm distance at the positive direction of Z axis, the distances at other axis directions are zero. Only the negative Z axis is set electric ($E_t=0$), the others are set magnetic ($H_t=0$). In Fig. 2(b), all the

distances of axis are 10mm, all the boundaries are set 'open'. In Fig. 2(c), all the distances are set zero and all the boundaries are set 'open'. In Fig. 2(d), the distances at X axis are set zero, distances of other axes are set 10mm, the boundaries are all set 'open'.

The four results of $S(1,1)$ s are shown in Fig. 3. The simulation accuracy are all set '-60dB'. The red line stands for the $S(1,1)$ of situation (a), the blue line stands for the $S(1,1)$ of situation (b), the yellow line stands for the $S(1,1)$ of situation (c) and the green line stands for the $S(1,1)$ of situation (d). The trends of the four curves are very similar, but their errors will increase at high frequencies such as above 4GHz. This can indicate to a certain extent that the FIT simulation is accurate, and the setting of boundary conditions has little effect on it.

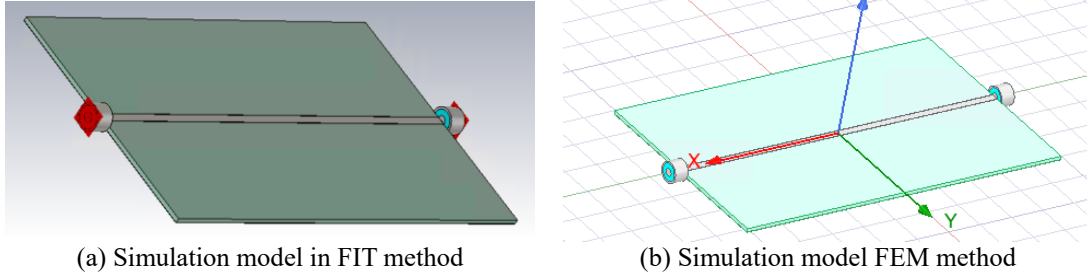


Fig. 4 Excitation setting in FIT method and FEM method

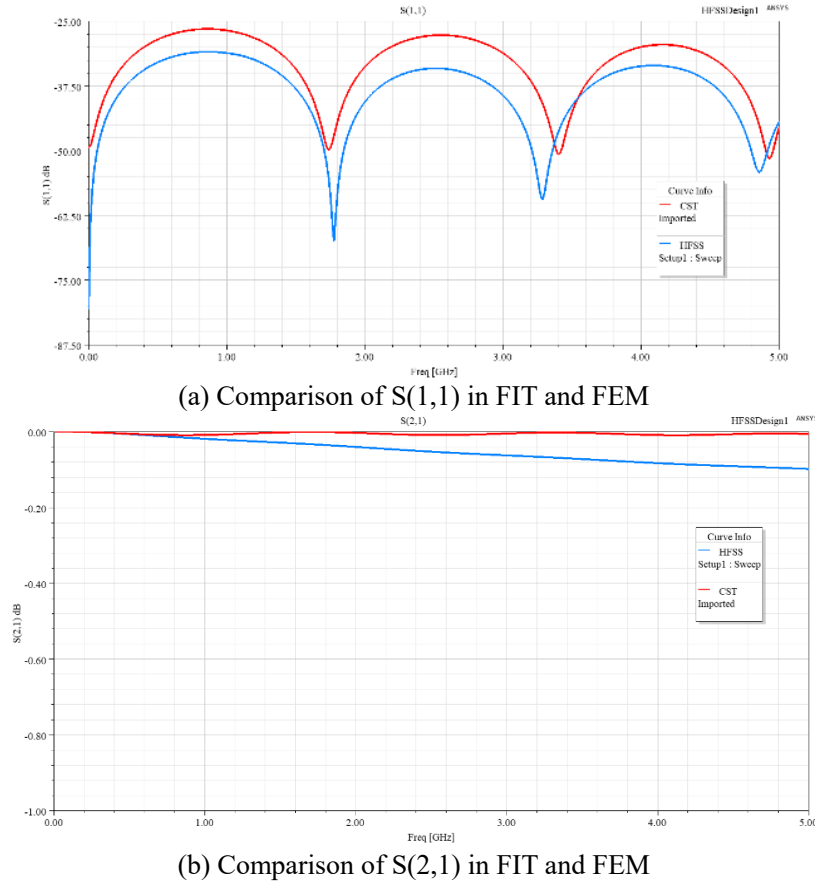


Fig. 5 S-parameters of cylindrical waveport in FIT and FEM

But for real application, the waveport can not be well applied, coaxial cable has to be connected to PCB

board for transferring. Now we consider to add a cylindrical waveguide on both sides of the microstripline. In that way, there won't be any difference in excitation. The models are shown in Fig. 4. even the simulations of 'thru' and 'line' are also very different in their magnitudes. In this section many kinds of boundary conditions are set to check the mistake, but the consistency of the materials for transmission line, substrate, ground are not carefully ensured.

The results in FIT and FEM are shown in Fig. 5. The red line stands for the curves in FIT, and the blue line stands for the curves in FEM. Due to the difference in algorithms between FIT and FEM, their simulation results can not be exactly the same especially in a multi-port simulation, but the result can be accepted.

2.1.2 Microstrip Antenna

The microstrip antenna is a simple radiator, there is only one feed point in this model. The material of the small cylinder is PEC, the substrate is made of RO4350, the patch and the low surface of substrate are set 'PerE' to perform as ground. The excitation is lumped port under the substrate at the feed point. The model of FIT method and FEM method are shown in Fig. 6. The boundary in FIT method is set 'open', the boundary in FEM method is set 'radiation'.

The circuit simulator schematic is shown in Fig. 7, the results are shown in Fig. 8, it shows that the two curves are very similar, the resonant frequencies are very close. That indicates the simulations are accurate. In this subsection, the simulation results of reflection coefficient for microstrip antenna in both FIT & FEM have a good agreement, that indicates the simulation is reasonable, to verify the simulation in another software or another algorithm is also a method to guarantee the simulation result.

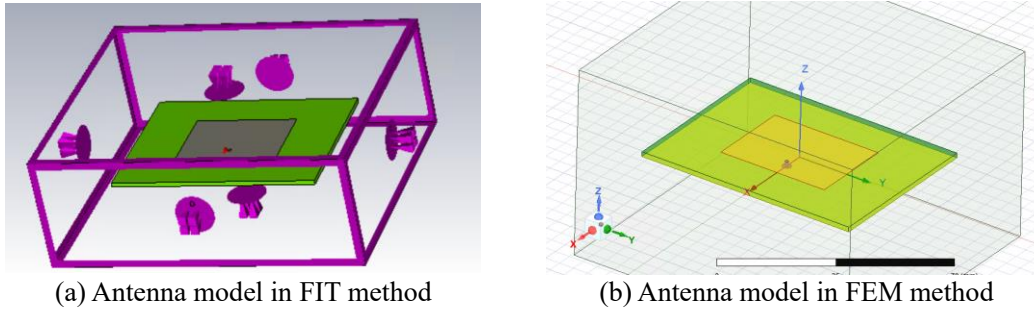


Fig. 6 The model of microstrip antenna for 3D full-wave simulation

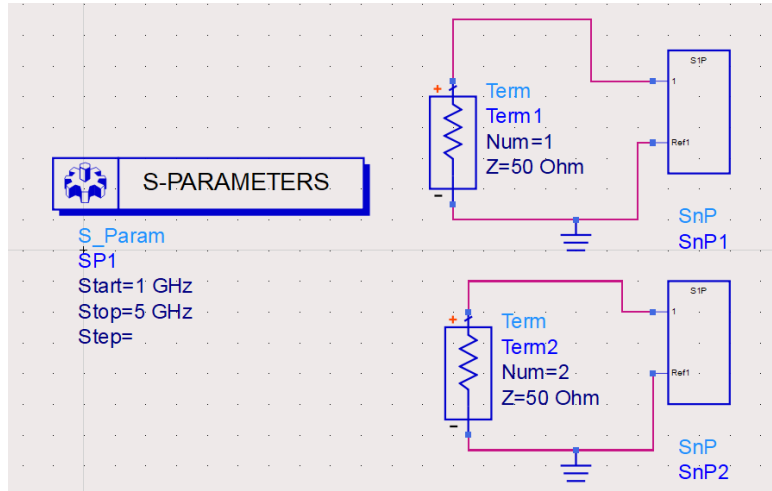


Fig. 7 Circuit simulator schematic of simulation for antenna

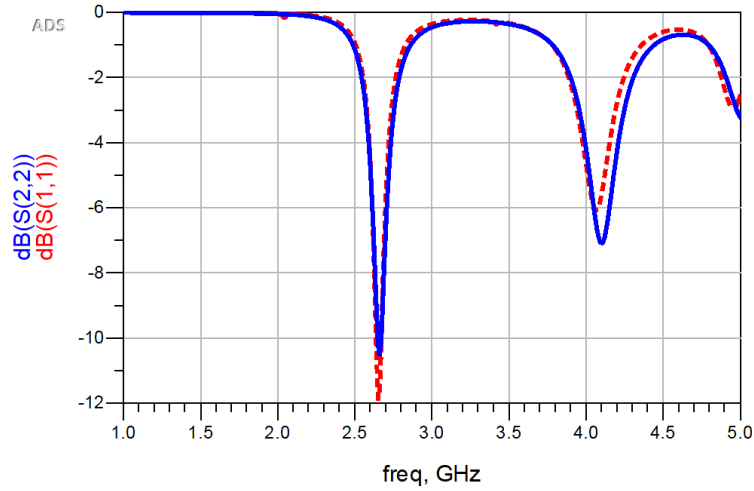


Fig. 8 Comparison of $S(1,1)$ for microstrip antenna (red for FIT method, blue for FEM method)

2.1.3 Bonding Wires

In this subsection, FIT method will only be utilized, a copper wire will be established to connect the gap of 'reflect' model in the subsection 2.1.3, here two copper wires are established in FIT method as shown in Fig. 9.

In this section the height of the wire is parameterized as h , h can be swept in simulation by a step width, in that way simulations can be automatically operated for many times and several results can be obtained. It is convenient for observing the influence of the specific parameter on the simulation. In this section, the parameter h is set from 0.5mm ~ 3.0mm by a step width 0.5mm.

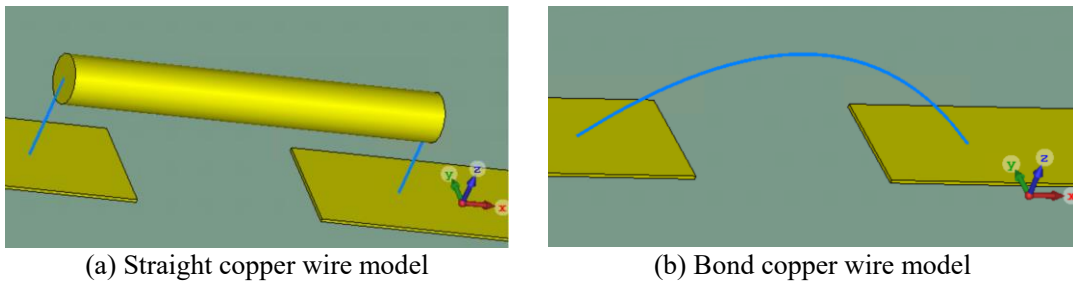
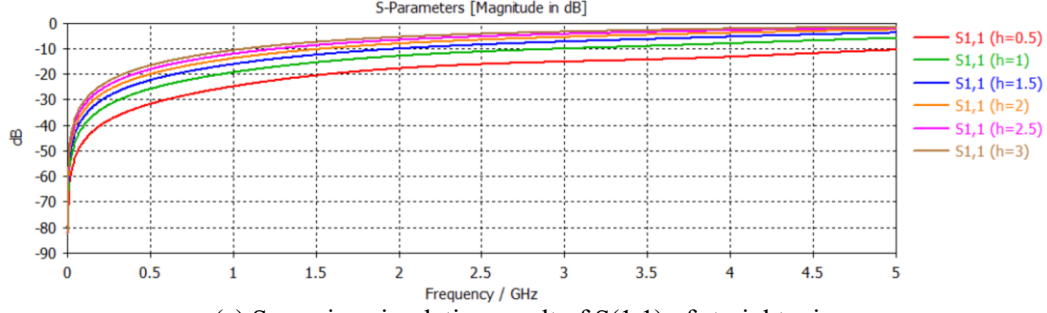


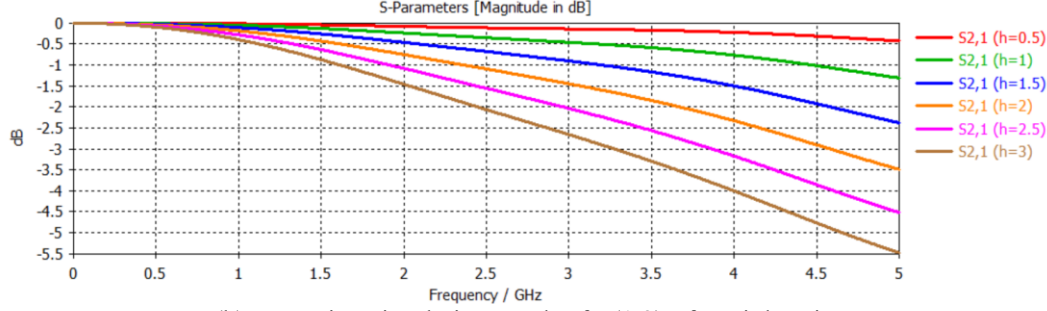
Fig. 9 Two copper wires in FIT working plane

The models corresponding to all the parameters will be simulated one by one (a), the reflection coefficient $S(1,1)$ s are presented in Fig. 10(a), the reverse transmission coefficient $S(1,2)$ s are shown in Fig. 10(b). From Fig. 10(b) it can be seen that as the height of copper wire increases, the whole length of wire increases, so the transmission loss also increases.

Sweeping simulation cannot only help observe the influence of parameter, but also to guarantee the plausibility of simulation.

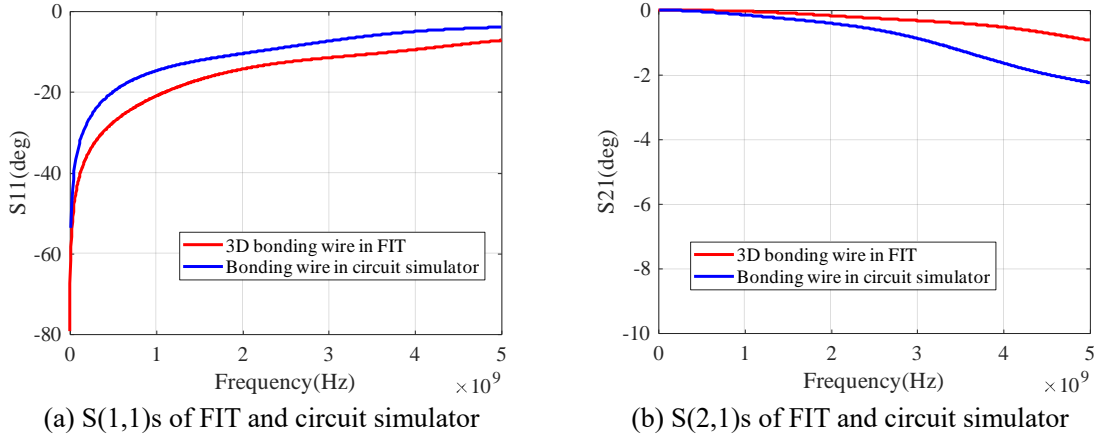


(a) Sweeping simulation result of S(1,1) of straight wire



(b) Sweeping simulation result of S(1,2) of straight wire

Fig. 10 S-parameters of straight copper wire



(a) S(1,1)s of FIT and circuit simulator

(b) S(2,1)s of FIT and circuit simulator

Fig. 11 Comparison of S-parameters for bonding wire

Circuit simulator can also be used to guarantee the reliability of simulation, for one situation in Fig. 9(b), the height is 1mm, so the whole length is 4.6mm, diameter is 0.5mm, then the inductance of bonding wire is about 2.66nH. The comparison result is shown in Fig. 11.

2.2 Calculation of Complex Permittivity

A new transmission line method for measuring the complex permittivity of dielectric materials using propagation constant measurements is presented[18]. The method will be referenced for calculation training, meanwhile the experiment equipment support at TET institute is enough.

First, the two 'touchstone.file' are obtained by FIT method simulation. Then the data is imported into MATLAB, the M' is obtained by

$$M^i = \frac{1}{S_{21_i}} \begin{bmatrix} (S_{12_i} S_{21_i} - S_{11_i} S_{22_i}) & S_{11_i} \\ -S_{22_i} & 1 \end{bmatrix} \quad (2-1)$$

M^{ij} is obtained by

$$M^{ij} = M^j [M^i]^{-1} \quad (2-2)$$

the two eigenvalues λ_{1M}^{ij} and λ_{2M}^{ij} of M^{ij} are obtained by

$$\lambda_{1M}^{ij}, \lambda_{2M}^{ij} = \frac{(M_{11}^{ij} + M_{22}^{ij}) \pm \sqrt{(M_{11}^{ij} - M_{22}^{ij})^2 + 4M_{12}^{ij}M_{21}^{ij}}}{2} \quad (2-3)$$

λ^{ij} is the average of the two eigenvalues as

$$\lambda^{ij} = \frac{1}{2} \left[\lambda_{1M}^{ij} + \lambda_{2M}^{ij} \right] \quad (2-4)$$

then the propagation constant γ can be calculated by

$$\gamma = \frac{\ln(\lambda^{ij})}{l_i - l_j} \quad (2-5)$$

where $l_i=50\text{mm}$, $l_j=60\text{mm}$, they stand for the length of two transmission lines.

The complex propagation constant can be divided into its real and imaginary parts as

$$\gamma(\omega) = \alpha(\omega) + j\beta(\omega) \quad (2-6)$$

so its real part and imaginary part can be both extracted.

So the real part of the sample permittivity ϵ'_s can be obtained by

$$\epsilon'_s = \frac{\beta^2 + \left(\frac{\pi}{a}\right)^2}{\omega^2 \mu_0 \epsilon_0} \quad (2-7)$$

where a stands for the longer width of the waveguide, $\omega=2\pi f$ stands for the radian frequency, $\mu_0=1.25664 \times 10^{-6}$ H/m and $\epsilon_0=8.8542 \times 10^{-12}$ F/m stand for the free space permeability and permittivity respectively.

If the conductive losses in the metal waveguide is neglected, the imaginary part of the sample permittivity can be obtained by

$$\epsilon''_s = \frac{2\alpha\epsilon'_s}{k} \sqrt{1 - \left(\frac{\lambda}{2a}\right)^2} \quad (2-8)$$

where

$$\lambda = \frac{2\pi}{k} \quad (2-9)$$

and

$$k = \omega \sqrt{\mu_0 \epsilon_0 \epsilon'_s} \quad (2-10)$$

First we calculate the difference of phase factor β by assuming the real part $\epsilon'_s=2.9$. Then we export the ASCII file of two S(2,1)s from FIT method and calculate the difference between them in MATLAB.

The comparison is shown in Fig. 12(a), the blue line stands for the ΔPhase from assuming $\epsilon'_s=2.9$, the orange line stands for the ΔPhase in FIT method, it is obvious that their trends are the same but in FIT method the phase is restored when at one frequency point it reaches 2π .

Then we suspect the problem only exist in the calculation of imaginary part. For the imaginary part of a complex number, the phase will be wrapped after a change of more than 2π especially in square or Square root. So according to equation (2-3) the propagation constant will be wrong.

We can also directly obtain the β from S-matrix extracted from the original touchstone file, then get the

phase by β . The result can be observed in Fig. 12(b), it is obvious that there is a step in the phase around frequency 11.3GHz.

Since the imaginary part of S-matrix has some problem in the phase, so the calculation of propagation constant γ will be wrong. If we apply $\pm j2\pi$ to the eigenvalue λ^{ij} in equation (5), we can obtain part of the right result. The result is shown in Fig. 13, the real part permittivity is shown in Fig. 13(a) and the imaginary part is shown in Fig. 13(b). The blue line stands for $\lambda_{ij}-j2\pi$, the orange line stands for $\lambda_{ij}+j2\pi$. From Fig. 13(a) it can be seen that there is a step at around 9.4GHz and an oscillation at around 9.7GHz. If the oscillation is neglected, under 9.4GHz the $\lambda_{ij}-j2\pi$ can lead to the right result permittivity=2.9, upon 9.4GHz, the $\lambda_{ij}+j2\pi$ can lead to the right result. The enlarged picture of real part is shown in Fig. 14. The result only changes from 2.9~2.925, it can be considered as a constant.

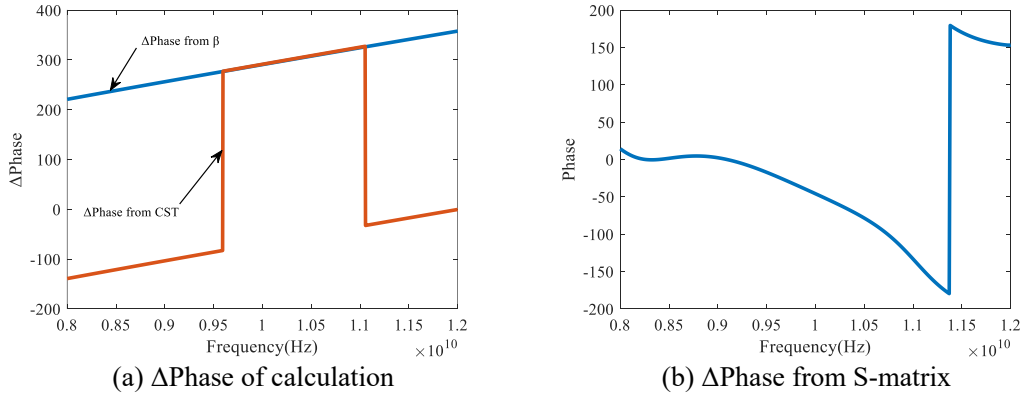


Fig. 12 Δ Phase of S(2,1)s

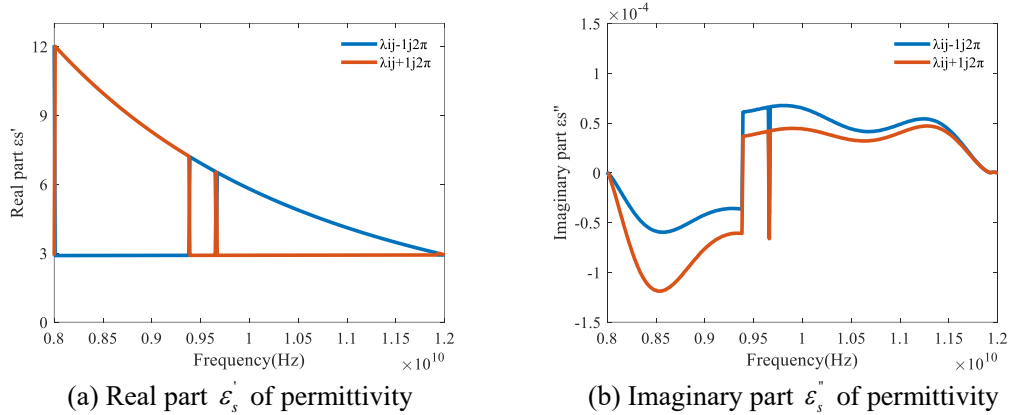


Fig. 13 Result of permittivity for $\lambda_{ij} \pm j2\pi$

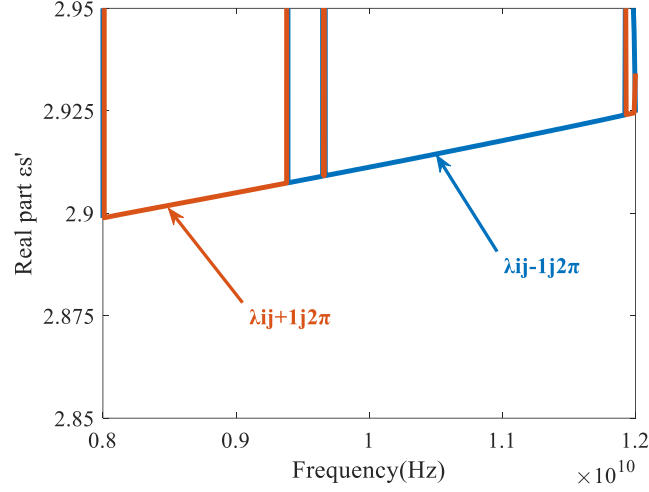


Fig. 14 Enlarged figure of real part of permittivity

The wrapping of phase is probably because of the difference of two lines. So in order to avoid the phase exceeding 2π to cause some error in the calculation, we consider to decrease the difference of lengths for the two waveguide transmission line.

The i line remains 25.4mm, the length of j line is changed to 20mm. The result is shown in Fig. 15. It is obvious that the real part of ϵ_s is close to 2.9 as set in FIT, the error is below 0.00345%. The result is good.

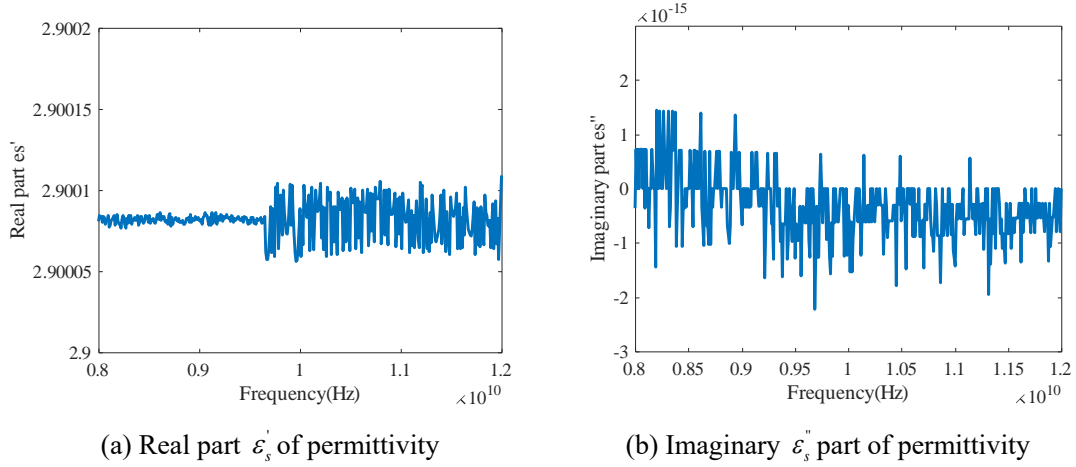


Fig. 15 Real part and imaginary part of permittivity

In this method of calculating the permittivity, the difference between the two waveguide transmission lines should not be too big, instead the smaller the better.

2.3 Measurement of Coaxial Cables

Other two coaxial cables are used as the Under Test Device, their data can be searched and found from the website[19][20][21], it is shown below in Table 2.

Table 2 Information of coaxial cables

No.	Label	Outside Diameter	Length	Velocity of Propagation	Signal Delay
1	Batch no. 1317297 ST18/SMAM/SMAM/48 Order no. 84003373	4.6mm	48in 1219.2mm	77%	4.3ns/m
2	Batch no. 2597910 ST18/SMAM/SMAM/72 Order no. 84004007	4.6mm	72in 1828.8mm	77%	4.3ns/m
3	Batch no. 2597910 ST18/SMAM/SMAM/36 Order no. 84002061	4.6mm	36in 914.4mm	77%	4.3ns/m

Now we try to simulate the coaxial cables in FIT method, from the document provided in the website, the velocity factor is 77%. So the the permittivity can be calculated by the velocity propagation through equation:

$$\text{VelocityFactor} = VF = \frac{1}{\sqrt{\mu_r \epsilon_r}} \quad (2-11)$$

So the $\epsilon_r=1.69$. We consider to use VNA experiment machine, MS46122B 20GHz Vector Network Analyzer from Anritsu Company, from 1MHz up to 18GHz to test the coaxial cable and observe the result. The VNA is shown in Fig. 16.



Fig. 16 Anritsu MS46122B VNA

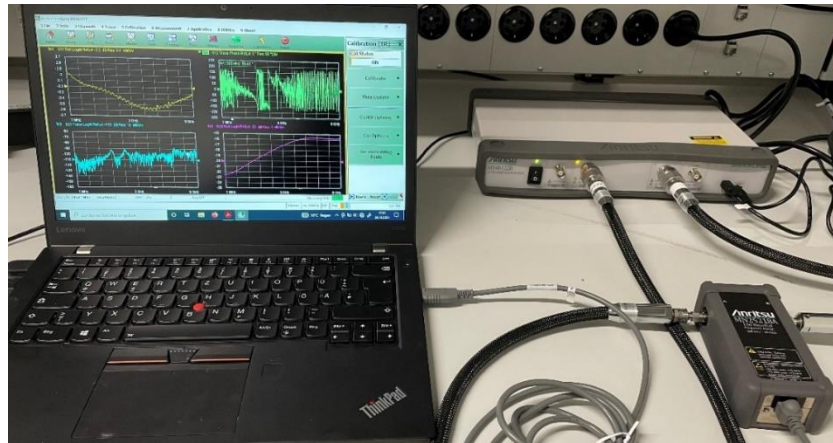


Fig. 17 Calibration of MS46122B VNA

The MS46122B VNA can be automatically calibrated by its calibrator body as shown in Fig. 17. After automatic calibration, the 48 inches coaxial cable is firstly tested so as to check the phase to observe if the data provided by the manufacture is believable or not. The screenshot of the S-parameter testing result is shown in Fig. 18.

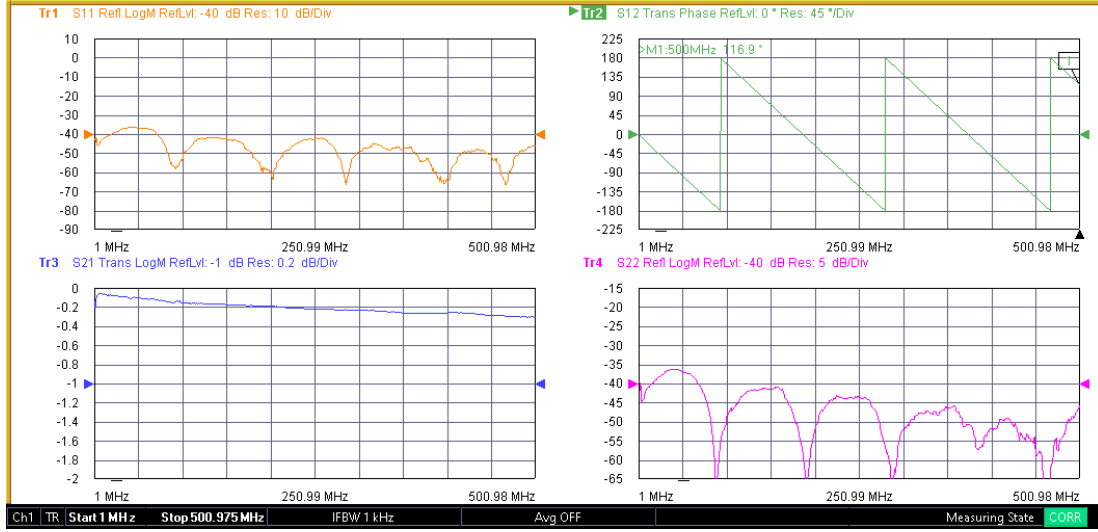
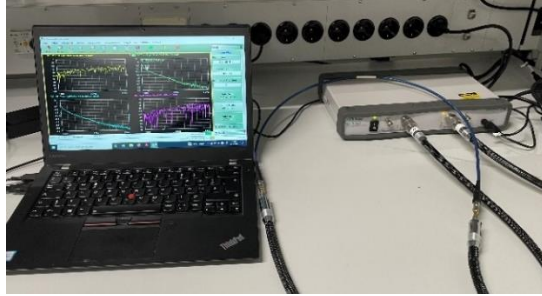


Fig. 18 Screenshot of the GUI for MS46122B VNA testing 48 inches coaxial cable

This time we measure the S-parameters of all three coaxial cables, their labels are shown in Fig. 19(a), the experimental scene is shown in Fig. 19(b). This time we measure the frequency range from 1MHz~6GHz.



(a) Three cables



(b) Experimental scene

Fig. 19 Cables and the measurement platform

The propagation constant can be calculated by measured S-parameters of two coaxial cables of different lengths, here we use the S-parameters of coaxial cable 36 inches and 72 inches, the result is shown in Fig. 20. It is obvious that the result is wrapping, we suspect that it is due to the large difference of length, the wrapping phase causes the wrapped result, the reason is already mentioned in section 2.2 and the solution is suggested to reduce the difference of lengths. But in this section, or in another way, when we only deal with the simulation result, the model is easy to adjust. But now we are focusing on the experiment and it is impossible to adjust the lengths as we wish.

The wrapping is caused at least three times in the program in MATLAB, once is the square root in equation (2-3), the twice is the phase wrapping of the result of propagation constant γ in equation (2-5).

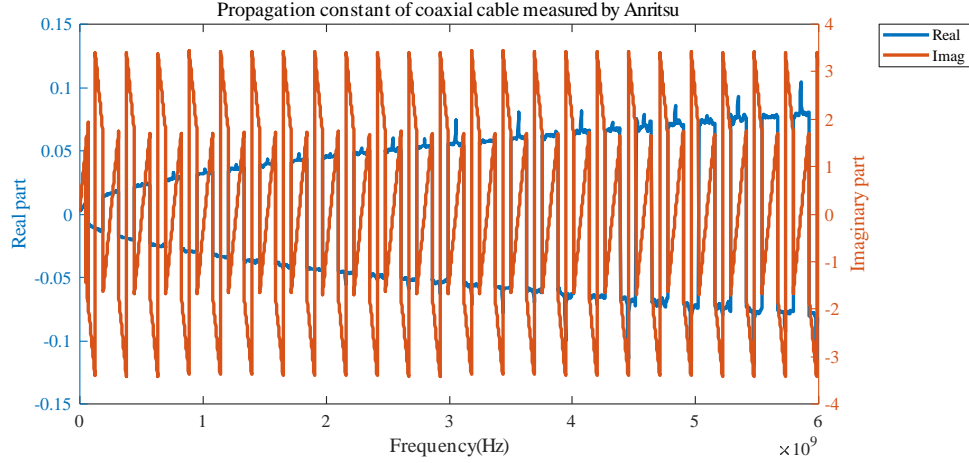


Fig. 20 The result caused by the wrapped phase

To prevent the imaginary part of propagation constant from wrapping, the code below is added in the extraction of β from γ . In addition, since the beta is monotonous, to prevent the result of beta from wrapping, the code below is added to ensure imaginary part β is right. After obtaining the β we can get the permittivity ϵ_r from equation (2-12) as shown below:

$$\epsilon_r = \left(\frac{\beta c_{\text{light}}}{\omega} \right)^2 \quad (2-12)$$

The relative permittivity will be obtained by the propagation constant. The result of propagation constant is shown in Fig. 21(a) and the relative permittivity is shown in Fig. 21(b). It is obvious that the real part and imaginary part change without wrapping, the permittivity decrease from about 1.8 and remains stable about 1.658 from 300MHz. The data indicates that the relative permittivity is 1.69, the error is about 1.9%.

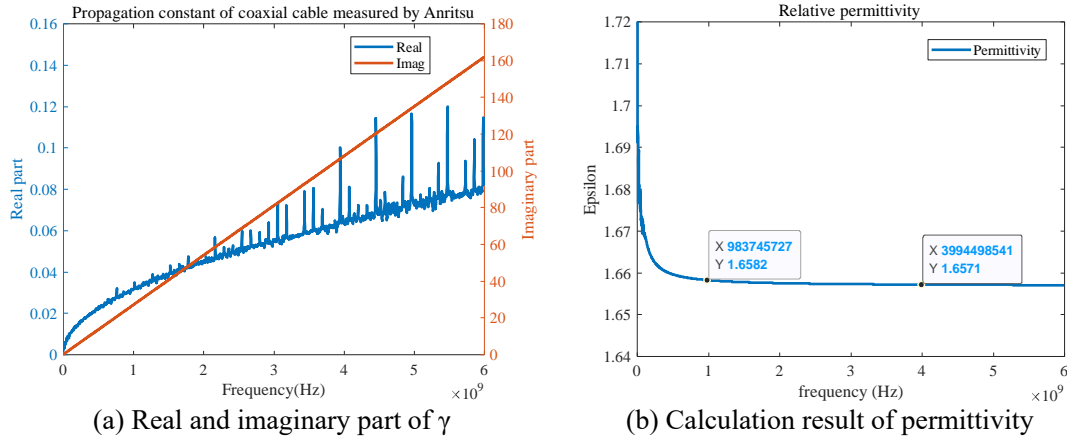


Fig. 21 Result of calculation for complex permittivity of coaxial transmission line

The reason of error may be the male connector added in the measurement because without two male connectors the two coaxial cables can not be connected to the VNA.

2.4 Summary

The work of this section enables the scholarship holder make a good preparation for the coming large number of simulation work in the following sections, and also improves the understanding of the three-dimensional full-wave electromagnetic field calculation. Some errors will be avoided and the efficiency

of simulation will be improved for the coming job related to the research proposal.

1. Due to the difference in algorithms between FIT and FEM, sometimes the simulation results can not be exactly the same especially in a multi-port simulation, but the result can be accepted, that depends on the 3D model, the frequency range. When the 3D model is complex, the FEM method will be more accurate, when implemented in the high frequency, the FIT method will be more accurate.
2. In some situation, sweeping simulation cannot only help observe the influence of parameter, but also to guarantee the plausibility of simulation. Through sweeping we can clearly observe the change of results, it helps to judge whether the result is reliable or not.
3. In this method of calculating the permittivity in subsection 2.2, the difference between the two waveguide transmission lines should not be too big, instead the smaller the better to avoid the wrapping of phase. But in real situation, the difference can not be as short as we wish, that is a common problem. Sometimes the simulation can be easily satisfied, but the actual situation cannot be satisfied. This requires adjustments to both the simulation and the actual measurement to make the two as consistent as possible.
4. In the measurement in subsection 2.3, the reason of error may be the male connector added in the measurement because without two male connectors the two coaxial cables can not be connected to the VNA. This is also a common problem in high frequency measurement or calibration, in the high frequency band, a small error of the calibration surface will lead to a phase deviation, resulting in a mismatch between the simulation and the actual measurement.

3 TRL Calibration Theory and Practice

Before researching and applying the TRL method, it is necessary to study the standard of the calibration method in the industry first. Such standards are formulated by experts in the electromagnetics industry and a standard for judging whether the calibration effect is reliable or not is given.

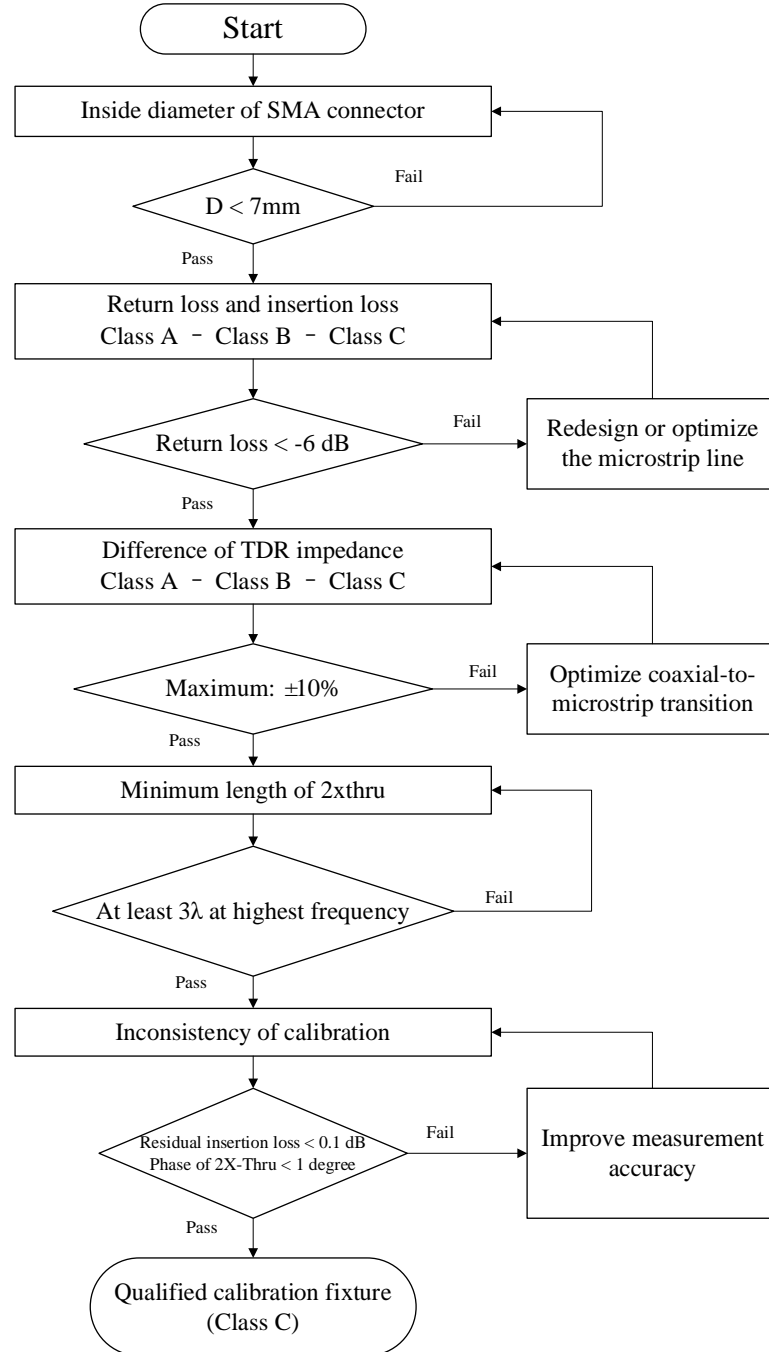


Fig. 22 Flow chart of standard process for fixture design in this article according to IEEE Standard 370

IEEE has evaluation standards for calibration methods, and this set of evaluation standards is based on the '2xthru' method, which provides recommended ranges for transmission line lengths at certain frequencies,

dimensions of coaxial microstrip adapters, and amplitudes of S-parameters. "2xthru" is the basic calibration method, and the requirements apply to more complex fixture designs, such as 'line' and 'DUT' in TRL fixtures.

In clause 3.3 of IEEE Standard 370-2020[22], the inside diameter of coaxial connector measured up to 18GHz should be lower than 7mm. If the SMA adaptor is with lower precision and non-air dielectrics, it can still be used but an additional adapter is required to be added. In the measurement of this article, a high precision female-to-male adapter is added between the coaxial cable and the SMA adaptor.

Since the fixture cannot be perfect and lossless, so in clause 4.3, the standard also proposes the requirements classes A, B and C for the performance of fixture, i.e. the transition of the fixture must not be too bad. A fixture is considered to be not qualified for all frequencies higher than the frequency of its first class C failure. In subclause 4.3.8, the standard also proposes a series of classes for the requirement of impedance transmission line measured by TDR method. To meet the requirement of class C, the difference from the reference impedance should be no high than 10%. In subclause 4.3.11, there is also a restriction for the minimum length of '2xthru', it should be at least three wavelength at the highest frequency. Also considering about the twisting of long PCB board during measurement, the 'line' will be set 50mm in this paper.

There must be inconsistency in the measurement of fixture, even if the measurements are operated at the same situation. So there will also be inconsistency after different calibrations. In clause 6.5, the IEEE Standard also states the error range for consistency of multiple calibrations. For a reliable '2xthru' fixture, the criteria of the maximum acceptable difference for the magnitude of insertion loss is no higher than 0.1dB, while the phase is no higher than 1 degree. The flow chart of process for TRL fixture design based on IEEE Std 370TM-2020 is shown in Fig. 22.

3.1 Derivation

In this section, all the equations about TRL calibration will be derivated in detail. All the variable written format will be corrected because whether the superscript or subscript of the variable is italicized in the reference is not rigorous[23].

Using T parameters (transfer parameters), we can show that if

$$\begin{cases} b_1 = S_{11}a_1 + S_{12}a_2 \\ b_2 = S_{21}a_1 + S_{22}a_2 \end{cases} \quad (3-1)$$

That is because

$$\begin{bmatrix} b_1 \\ b_2 \end{bmatrix} = \begin{bmatrix} S_{11} & S_{12} \\ S_{21} & S_{22} \end{bmatrix} \begin{bmatrix} a_1 \\ a_2 \end{bmatrix} \Rightarrow \begin{cases} b_1 = S_{11} \cdot a_1 + S_{12} \cdot a_2 \\ b_2 = S_{21} \cdot a_1 + S_{22} \cdot a_2 \end{cases} \quad (3-2)$$

So we can extract

$$a_1 = \frac{b_2 - S_{22}a_2}{S_{21}} \quad (3-3)$$

Take equation (3-3) into equation (3-2) we can have

$$b_1 = S_{11} \cdot \frac{b_2 - S_{22}a_2}{S_{21}} + S_{12}a_2 = \frac{S_{11} \cdot b_2 - S_{11} \cdot S_{22} \cdot a_2 + S_{12} \cdot S_{21} \cdot a_2}{S_{21}} \quad (3-4)$$

So we can have

$$\begin{pmatrix} b_1 \\ a_1 \end{pmatrix} = \frac{1}{S_{21}} \begin{pmatrix} -(S_{11}S_{22} - S_{12}S_{21}) & S_{11} \\ -S_{22} & 1 \end{pmatrix} \begin{pmatrix} a_2 \\ b_2 \end{pmatrix} = \frac{1}{S_{21}} \begin{pmatrix} -\Delta & S_{11} \\ -S_{22} & 1 \end{pmatrix} \begin{pmatrix} a_2 \\ b_2 \end{pmatrix}, \Delta = S_{11}S_{22} - S_{12}S_{21} \quad (3-5)$$

There is a mistake in the slide 16th where the position of a_2 and b_2 is opposite. We can also have

$$R = \frac{1}{S_{21}} \begin{pmatrix} -\Delta & S_{11} \\ -S_{22} & 1 \end{pmatrix} \quad (3-6)$$

The measurement matrix R_M is just the result of the matrices of the error boxes and the unknown Device-Under-Test (DUT), so we can have

$$R_M = R_A R R_B \quad (R_{\text{measured}} = \text{MatrixA} \cdot \text{DUT} \cdot \text{MatrixB}) \quad (3-7)$$

or

$$R = R_A^{-1} R_M R_B^{-1} \quad (3-8)$$

Let R_A be written as

$$R_A = \begin{bmatrix} r_{11} & r_{12} \\ r_{21} & r_{22} \end{bmatrix} = r_{22} \begin{bmatrix} \frac{r_{11}}{r_{22}} & \frac{r_{12}}{r_{22}} \\ \frac{r_{21}}{r_{22}} & \frac{r_{22}}{r_{22}} \end{bmatrix} = r_{22} \begin{bmatrix} a & b \\ c & 1 \end{bmatrix} \quad (3-9)$$

and R_B can be similarly written as

$$R_B = \begin{bmatrix} \rho_{11} & \rho_{12} \\ \rho_{21} & \rho_{22} \end{bmatrix} = \rho_{22} \begin{bmatrix} \frac{\rho_{11}}{\rho_{22}} & \frac{\rho_{12}}{\rho_{22}} \\ \frac{\rho_{21}}{\rho_{22}} & \frac{\rho_{22}}{\rho_{22}} \end{bmatrix} = \rho_{22} \begin{bmatrix} \alpha & \beta \\ \gamma & 1 \end{bmatrix} \quad (3-10)$$

Obviously according to equation (3-9) the inverse matrix of R_A is

$$R_A^{-1} = \frac{1}{r_{22}} \begin{bmatrix} a & b \\ c & 1 \end{bmatrix}^{-1} = \frac{1}{r_{22}} \left\{ \frac{1}{(a \cdot 1 - b \cdot c)} \begin{bmatrix} 1 & -b \\ -c & a \end{bmatrix} \right\} = \frac{1}{r_{22}} \frac{1}{a - bc} \begin{bmatrix} 1 & -b \\ -c & a \end{bmatrix} \quad (3-11)$$

so according to (3-10) the inverse of R_B is

$$R_B^{-1} = \frac{1}{\rho_{22}} \begin{bmatrix} \alpha & \beta \\ \gamma & 1 \end{bmatrix}^{-1} = \frac{1}{\rho_{22}} \frac{1}{\alpha - \beta\gamma} \begin{bmatrix} 1 & -\beta \\ -\gamma & \alpha \end{bmatrix} \quad (3-12)$$

So taking equations (3-11), (3-12) into equation (3-8) we can have the matrix of DUT R as

$$R = \frac{1}{r_{22}} \frac{1}{a - bc} \begin{bmatrix} 1 & -b \\ -c & a \end{bmatrix} R_M \frac{1}{\rho_{22}} \frac{1}{\alpha - \beta\gamma} \begin{bmatrix} 1 & -\beta \\ -\gamma & \alpha \end{bmatrix} = \frac{1}{r_{22} \rho_{22}} \frac{1}{a\alpha} \frac{1}{1 - b\frac{c}{a} - \gamma\frac{\beta}{\alpha}} \begin{bmatrix} 1 & -b \\ -c & a \end{bmatrix} R_M \begin{bmatrix} 1 & -\beta \\ -\gamma & \alpha \end{bmatrix} \quad (3-13)$$

Note that although there are eight terms in the error boxes, only seven quantities are needed to be found to get matrix R , they are $a, b, c, \alpha, \beta, \gamma$ and $r_{22}\rho_{22}$.

From the measurement of the through and of the line, seven quantities will be obtained, let us find the above seven quantities.

The ideal through has an R matrix which is the 2×2 unit matrix. The measured R matrix with the through connected will be denoted by R_T and is given by

$$R_T = R_A R_B \quad (R_{\text{Thru}} = \text{MatrixA} \cdot \text{MatrixB}) \quad (3-14)$$

where R_A and R_B are the matrices of the error box A and B respectively. In the 'line' connection, the measured R matrix will be denoted by R_D and is equal to

$$R_D = R_A R_L R_B \quad (R_{\text{Delay}} = \text{MatrixA} \cdot R_{\text{Line}} \cdot \text{MatrixB}) \quad (3-15)$$

where R_L is the R matrix of the line, so from equation (3-14) there is

$$R_B = R_A^{-1} R_T \quad (3-16)$$

so that we can have

$$R_D = R_A R_L R_B = R_A R_L R_A^{-1} R_T \quad (3-17)$$

and so obviously we have

$$R_D R_T^{-1} R_A = R_A R_L \quad (3-18)$$

Let's define

$$T = R_D R_T^{-1} \quad (3-19)$$

and take equation (3-19) into (3-18) we have

$$TR_A = R_A R_L \quad (3-20)$$

Obviously the matrix T can be obtained from measurements 'Thru' and 'Line' and it can be written as

$$T = \begin{bmatrix} t_{11} & t_{12} \\ t_{21} & t_{22} \end{bmatrix} \quad (3-21)$$

Assuming the line is non-reflecting we have the R_L matrix

$$R_L = \begin{bmatrix} e^{-\gamma l} & 0 \\ 0 & e^{+\gamma l} \end{bmatrix} \quad (3-22)$$

Matrices R_A and R_B are unknown and were able to be written as

$$\begin{cases} R_A = \begin{bmatrix} r_{11} & r_{12} \\ r_{21} & r_{22} \end{bmatrix} = r_{22} \begin{bmatrix} a & b \\ c & 1 \end{bmatrix} \\ R_B = \begin{bmatrix} \rho_{11} & \rho_{12} \\ \rho_{21} & \rho_{22} \end{bmatrix} = \rho_{22} \begin{bmatrix} \alpha & \beta \\ \gamma & 1 \end{bmatrix} \end{cases} \quad (3-23)$$

Recalling equation (3-20) and here write the matrices results in below

$$\begin{bmatrix} t_{11} & t_{12} \\ t_{21} & t_{22} \end{bmatrix} \begin{bmatrix} a & b \\ c & 1 \end{bmatrix} = \begin{bmatrix} a & b \\ c & 1 \end{bmatrix} \begin{bmatrix} e^{-\gamma l} & 0 \\ 0 & e^{+\gamma l} \end{bmatrix} \quad (3-24)$$

So calcite the equation (3-24) we can have

$$\begin{bmatrix} t_{11} \cdot a + t_{12} \cdot c & t_{11} \cdot b + t_{12} \cdot 1 \\ t_{21} \cdot a + t_{22} \cdot c & t_{21} \cdot b + t_{22} \cdot 1 \end{bmatrix} = \begin{bmatrix} a \cdot e^{-\gamma l} + b \cdot 0 & a \cdot 0 + b \cdot e^{+\gamma l} \\ c \cdot e^{-\gamma l} + 1 \cdot 0 & c \cdot 0 + 1 \cdot e^{+\gamma l} \end{bmatrix} \quad (3-25)$$

that is

$$\begin{bmatrix} t_{11}a + t_{12}c & t_{11}b + t_{12} \\ t_{21}a + t_{22}c & t_{21}b + t_{22} \end{bmatrix} = \begin{bmatrix} ae^{-\gamma l} & be^{+\gamma l} \\ ce^{-\gamma l} & e^{+\gamma l} \end{bmatrix} \quad (3-26)$$

so that gives four equations as (3-27) ~ (3-30)

$$t_{11}a + t_{12}c = ae^{-\gamma l} \quad (3-27)$$

$$t_{21}a + t_{22}c = ce^{-\gamma l} \quad (3-28)$$

$$t_{11}b + t_{12} = be^{+\gamma l} \quad (3-29)$$

$$t_{21}b + t_{22} = e^{+\gamma l} \quad (3-30)$$

Dividing equation (3-27) by (3-28) results in

$$\frac{t_{11}a + t_{12}c}{t_{21}a + t_{22}c} = \frac{ae^{-\gamma l}}{ce^{-\gamma l}} \Rightarrow \frac{t_{11}a + t_{12}c}{t_{21}a + t_{22}c} = \frac{a}{c} = \frac{t_{11} \frac{a}{c} + t_{12}}{t_{21} \frac{a}{c} + t_{22}} \quad (3-31)$$

and equation (3-31) is equal to a quadratic equation for a/c as

$$t_{21} \left(\frac{a}{c} \right)^2 + (t_{22} - t_{11}) \frac{a}{c} - t_{12} = 0 \quad (3-32)$$

Dividing equation (3-29) by (3-30) results in

$$\frac{t_{11}b + t_{12}}{t_{21}b + t_{22}} = \frac{be^{+\gamma l}}{e^{+\gamma l}} \Rightarrow \frac{t_{11}b + t_{12}}{t_{21}b + t_{22}} = b \quad (3-33)$$

and equation (3-30) is equal to an analogous quadratic equation for b as

$$t_{21}b^2 + (t_{22} - t_{11})b - t_{12} = 0 \quad (3-34)$$

Diving equation (3-30) by (3-28) results in

$$\frac{t_{21}b+t_{22}}{t_{21}a+t_{22}c} = \frac{e^{+\gamma l}}{ce^{-\gamma l}} \Rightarrow e^{2\gamma l} = c \frac{t_{21}b+t_{22}}{t_{21}a+t_{22}c} = \frac{t_{21}b+t_{22}}{t_{21}\frac{a}{c}+t_{22}} \quad (3-35)$$

Since $e^{2\gamma l}$ can not be equal to 1, b and $\frac{a}{c}$ are distinct roots of the quadratic equation. So the choice of the root will be discussed now. Obviously according to equation (3-9)

$$b = \frac{r_{12}}{r_{22}} = S_{11} \quad (3-36)$$

According to equation (3-6)

$$\frac{a}{c} = \frac{r_{11}}{r_{21}} = \frac{-\Delta}{-S_{22}} = \frac{S_{11}S_{22} - S_{12}S_{21}}{S_{22}} = S_{11} - \frac{S_{12}S_{21}}{S_{22}} \quad (3-37)$$

And for a well designed transmission line $|S_{22}|, |S_{11}| \ll 1$ which yields $|b| \ll 1$ and $\left|\frac{a}{c}\right| \gg 1$, so $|b| \ll \left|\frac{a}{c}\right|$

which determines the choice of the root.

Recalling equation (3-20) we have

$$TR_A = R_A R_L \Rightarrow (\det T)(\det R_A) = (\det R_A)(\det R_L) \quad (3-38)$$

According to equation (3-22) we have

$$(\det R_L) = e^{-\gamma l} \cdot e^{+\gamma l} = 1 \quad (3-39)$$

so taking (3-39) to (3-38) we can have

$$(\det T) = (\det R_L) = 1 \quad (3-40)$$

so that

$$t_{11}t_{22} - t_{12}t_{21} = 1 \quad (3-41)$$

According to equation (3-14) we have

$$R_A R_B = r_{22} \rho_{22} \begin{bmatrix} a & b \\ c & 1 \end{bmatrix} \begin{bmatrix} \alpha & \beta \\ \gamma & 1 \end{bmatrix} = R_T = g \begin{bmatrix} d & e \\ f & 1 \end{bmatrix} \quad (3-42)$$

According to (3-11) we have

$$\begin{bmatrix} a & b \\ c & 1 \end{bmatrix}^{-1} = \frac{1}{a-bc} \begin{bmatrix} 1 & -b \\ -c & a \end{bmatrix} \quad (3-43)$$

Taking equation (3-43) to (3-42) we have

$$r_{22} \rho_{22} \begin{bmatrix} \alpha & \beta \\ \gamma & 1 \end{bmatrix} = \frac{g}{a-bc} \begin{bmatrix} 1 & -b \\ -c & a \end{bmatrix} \begin{bmatrix} d & e \\ f & 1 \end{bmatrix} \quad (3-44)$$

or

$$r_{22} \rho_{22} \begin{bmatrix} \alpha & \beta \\ \gamma & 1 \end{bmatrix} = \frac{g}{a-bc} \begin{bmatrix} d-bf & e-b \\ af-cd & a-ce \end{bmatrix} \quad (3-45)$$

because from equation (3-45) we can know

$$r_{22} \rho_{22} \begin{bmatrix} \alpha & \beta \\ \gamma & 1 \end{bmatrix} = \frac{g(a-ce)}{a-bc} \begin{bmatrix} \frac{d-bf}{a-ce} & \frac{e-b}{a-ce} \\ \frac{af-cd}{a-ce} & 1 \end{bmatrix} \quad (3-46)$$

so obviously we can have

$$r_{22} \rho_{22} = g \frac{a-ce}{a-bc} = g \frac{1-e\frac{c}{a}}{1-b\frac{c}{a}} \quad (3-47)$$

and

$$r \begin{bmatrix} \alpha & \beta \\ \gamma & 1 \end{bmatrix} = \frac{1}{a-bc} \begin{bmatrix} d-bf & e-b \\ af-cd & a-ce \end{bmatrix} \quad (3-48)$$

so we can also obtain quantities

$$\gamma = \frac{f - \frac{c}{a}d}{1 - \frac{c}{a}e} \quad (3-49)$$

$$\frac{\beta}{\alpha} = \frac{e-b}{d-bf} \quad (3-50)$$

$$\alpha a = \frac{d-bf}{1 - \frac{c}{a}e} \quad (3-51)$$

To complete the solution, one needs to find a , let the reflection measurement through error box A be w_1

$$w_1 = \frac{a\Gamma_R + b}{c\Gamma_R + 1} \quad (3-52)$$

which may be solved for a in terms of the known b and a/c as

$$w_1 c \Gamma_R + w_1 = a \Gamma_R + b \Rightarrow w_1 - b = a \Gamma_R \left(1 - \frac{w_1 c}{a} \right) \Rightarrow a = \frac{w_1 - b}{\Gamma_R \left(1 - w_1 \frac{c}{a} \right)} \quad (3-53)$$

we need a method to determine a . Use the measurement for the reflect from through the error box B. Let w_2 denote the measurement

$$w_2 = S_{22} + \frac{S_{12}S_{21}\Gamma_R}{1 - S_{11}\Gamma_R} = \frac{S_{22} - (S_{11}S_{22} - S_{12}S_{21})\Gamma_R}{1 - S_{11}\Gamma_R} = \frac{S_{22} - \Delta\Gamma_R}{1 - S_{11}\Gamma_R} \quad (3-54)$$

According to equation (3-23) we have

$$w_2 = \frac{-\frac{\rho_{21}}{\rho_{22}} + \frac{\rho_{11}}{\rho_{22}} \Gamma_R}{1 - \frac{\rho_{12}}{\rho_{22}} \Gamma_R} \quad (3-55)$$

or

$$w_2 = \frac{\alpha\Gamma_R - \gamma}{\beta\Gamma_R - 1} \quad (3-56)$$

so from equation (3-56) a may be found in terms of γ and β/a as

$$w_2 \beta \Gamma_R - w_2 = \gamma - \alpha \Gamma_R \Rightarrow \left(w_2 \frac{\beta}{\alpha} + 1 \right) \Gamma_R = \frac{\gamma + w_2}{\alpha} \Rightarrow \alpha = \frac{w_2 + \gamma}{\Gamma_R \left(1 + w_2 \frac{\beta}{\alpha} \right)} \quad (3-57)$$

Recalling equation (3-53) so that we have

$$\frac{a}{\alpha} = \frac{\frac{w_1 - b}{\Gamma_R \left(1 - w_1 \frac{c}{a} \right)}}{\frac{w_2 + \gamma}{\Gamma_R \left(1 + w_2 \frac{\beta}{\alpha} \right)}} = \frac{w_1 - b}{w_2 + \gamma} \frac{1 + w_2 \frac{\beta}{\alpha}}{1 - w_1 \frac{c}{a}} \quad (3-58)$$

Recalling equation (3-51) we can have

$$a^2 = \frac{w_1 - b}{w_2 + \gamma} \frac{1 + w_2}{1 - w_1} \frac{\beta}{\alpha} \frac{d - bf}{1 - \frac{c}{a} e} \quad (3-59)$$

or

$$a = \pm \left(\frac{w_1 - b}{w_2 + \gamma} \frac{1 + w_2}{1 - w_1} \frac{\beta}{\alpha} \frac{d - bf}{1 - \frac{c}{a} e} \right)^{\frac{1}{2}} \quad (3-60)$$

which determine a to within a \pm sign, recalling equation (3-53) that if Γ_R is known to within \pm then a may be determined as well. Calibration is complete and we can now proceed to the measurement of the DUT. From earlier the matrix of DUT is found from equation (3-13)

$$R = \frac{1}{r_{22}\rho_{22}} \frac{1}{a\alpha} \frac{1}{1-b\frac{c}{a}} \frac{1}{1-\gamma\frac{\beta}{\alpha}} \begin{bmatrix} 1 & -b \\ -c & a \end{bmatrix} R_M \begin{bmatrix} 1 & -\beta \\ -\gamma & \alpha \end{bmatrix} \quad (3-61)$$

in which all the terms have now been determined.

Now the derivation of TRL calibration is finished in such a detail progress.

3.2 Implementation

In this section the TRL calibration method will be implemented by simulation data, simulation situation will change from simple to complex.

3.2.1 Implementation of Section 2.1.1

Now we will use the data in the subsection 2.1.1 for TRL calibration. The 'Thru', 'Reflect', 'Line' data is obtained from a microstrip line. The 'DUT' is simulated by a serial element of which the resistance is 5Ω and the capacitance is $1\mu F$. The comparison of $S(1,1)$ and $S(2,1)$ before and after TRL calibration is shown in Fig. 23.

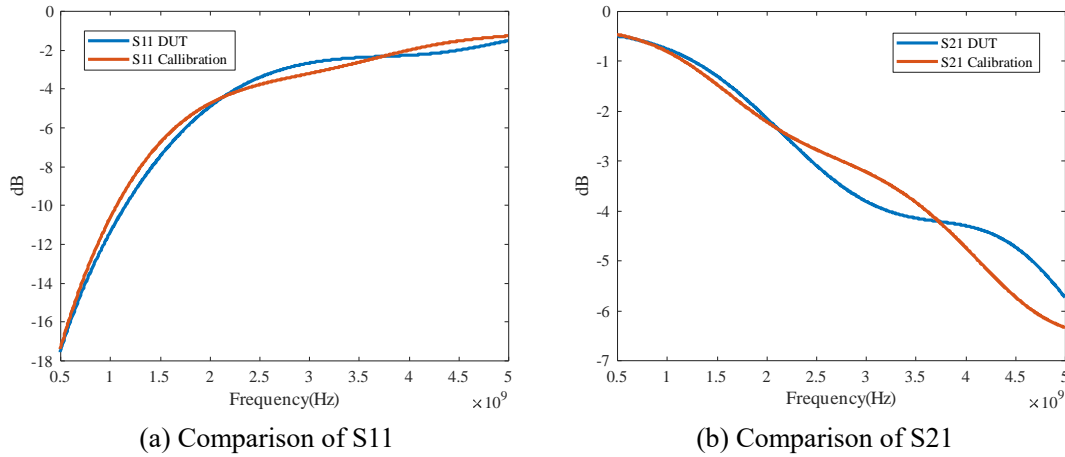


Fig. 23 Comparison of $S(1,1)$ and $S(2,1)$ for before and after calibration

The comparison of the phase of $S(1,1)$ and $S(2,1)$ is shown in Fig. 24.

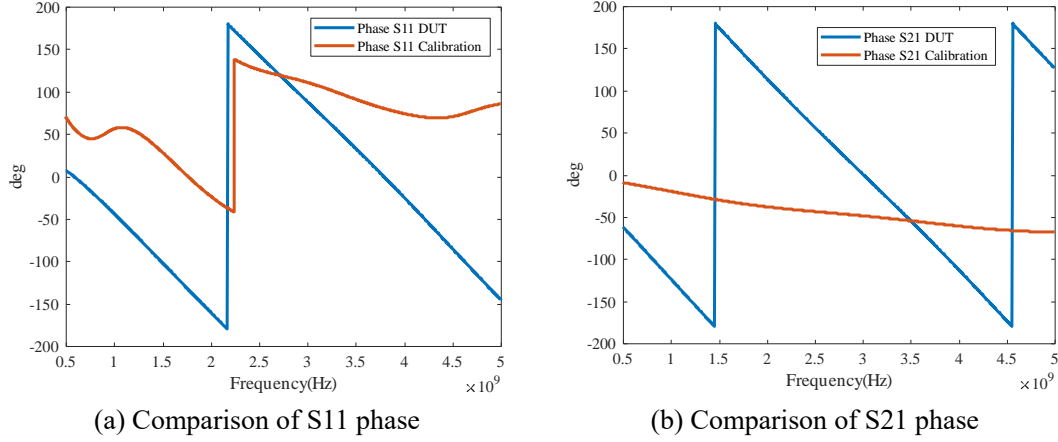


Fig. 24 Comparison of phase for S(1,1) and S(2,1) for before and after calibration

3.2.2 Implementation without SMA Connector

The remained detail simulation and comparison of R/L/C element as DUT in microstrip line will be continued. The whole length of transmission line is 50mm, the excitation is two discrete ports, the gap and the length of DUT is 2mm as shown in Fig. 25(a). The R/L/C is set as $1\text{m}\Omega$, 50Ω , $10\text{k}\Omega$, $1\mu\text{H}$, 1nH , 1fH , $1\mu\text{F}$, 1pF , 1fF , respectively.

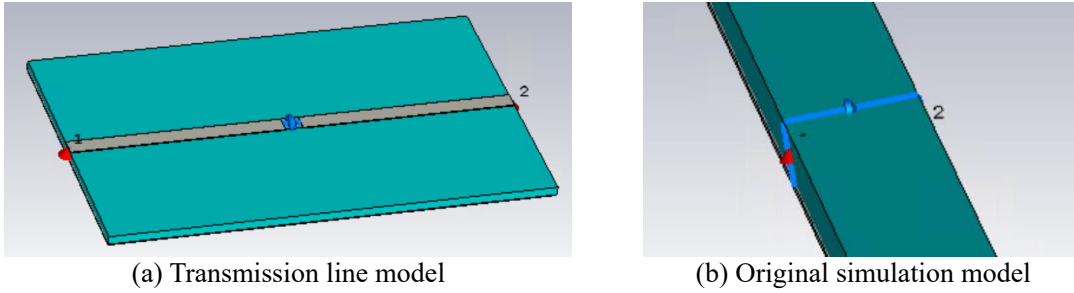


Fig. 25 Simulation model of microstrip line and DUT without trace

To prepare for the reference/original data of an R/L/C element, the S-parameter of the element will be simulated by cutting off the transmission line with only the element left as shown in Fig. 25(b).

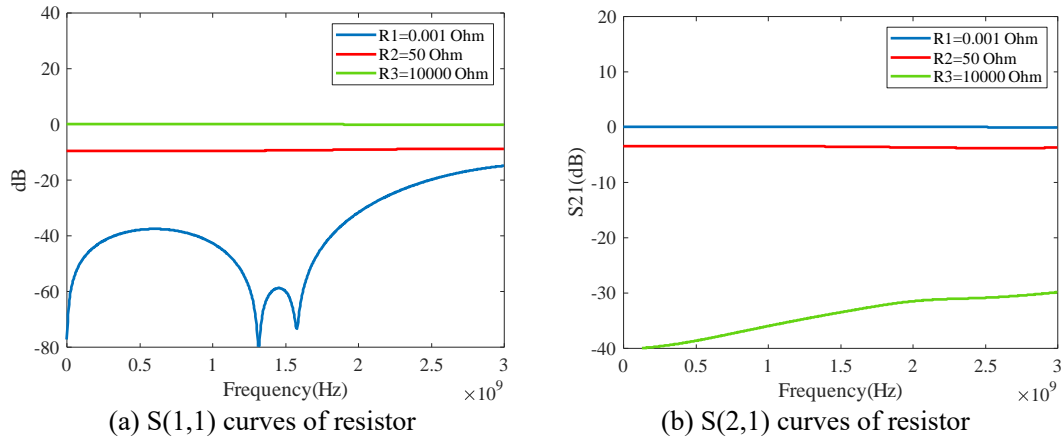


Fig. 26 Comparison of resistance element

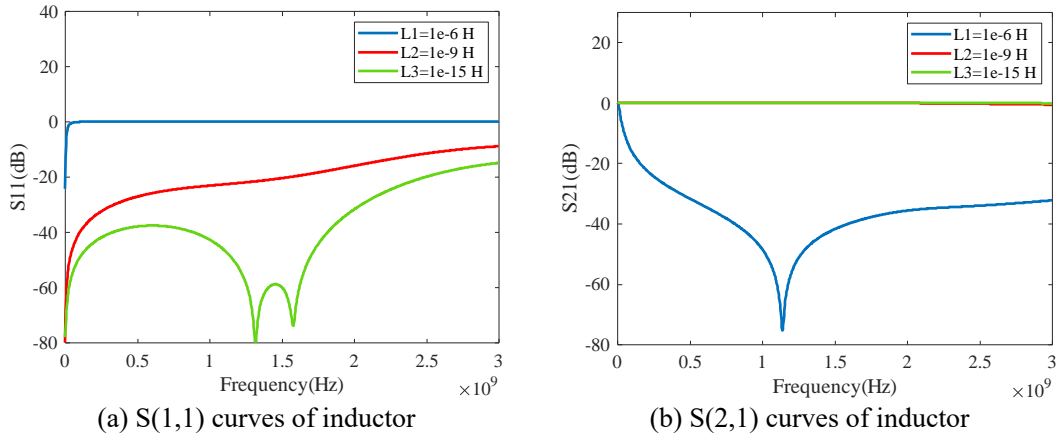


Fig. 27 Comparison of inductance element

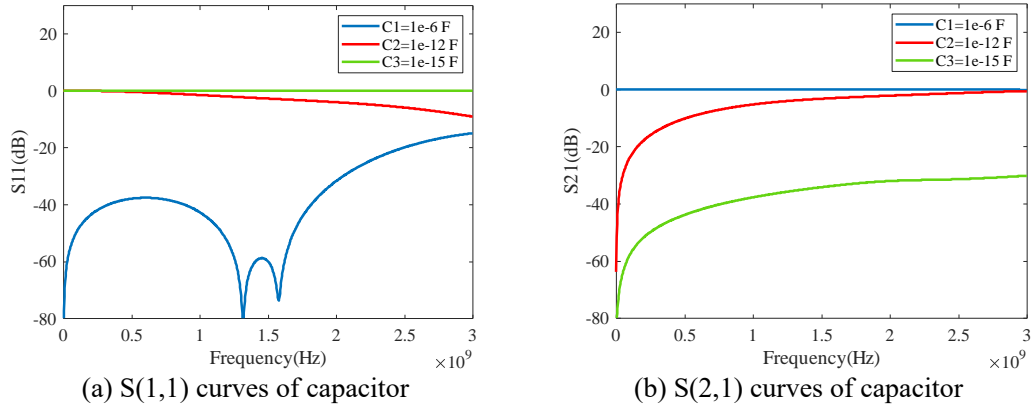


Fig. 28 Comparison of capacitance element

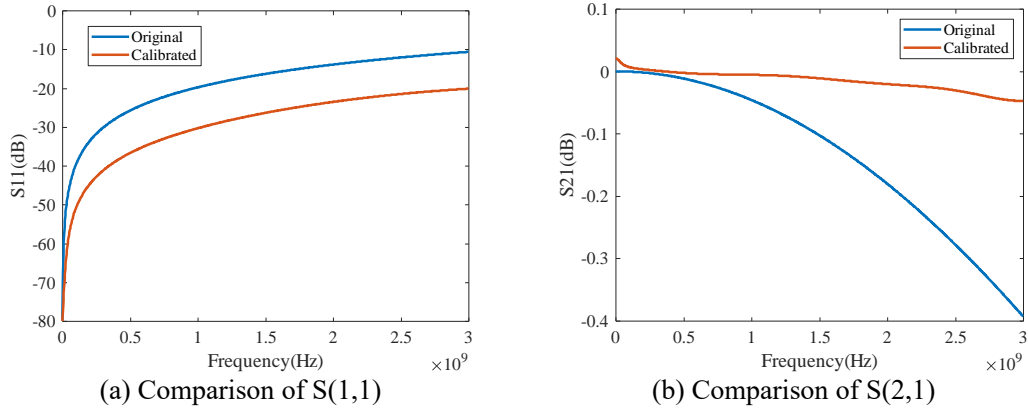


Fig. 29 The comparison between original and calibrated result of $R=0.001\Omega$

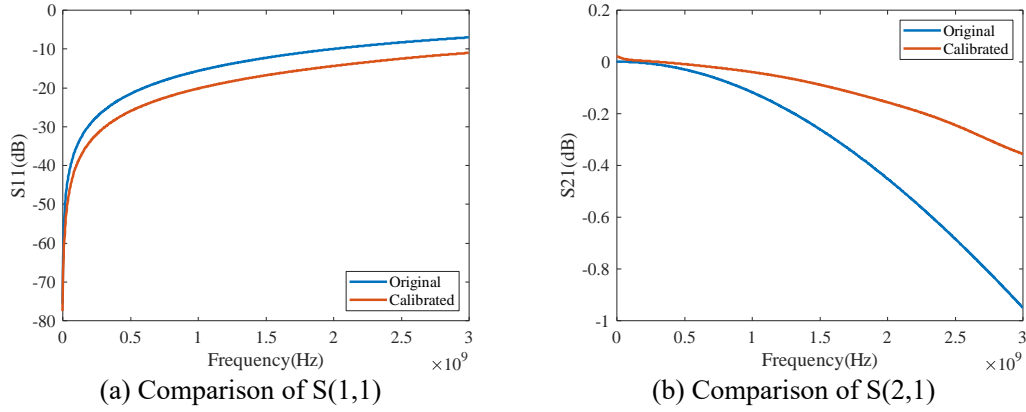


Fig. 30 The comparison between original and calibrated result of $L=1e-9$ H

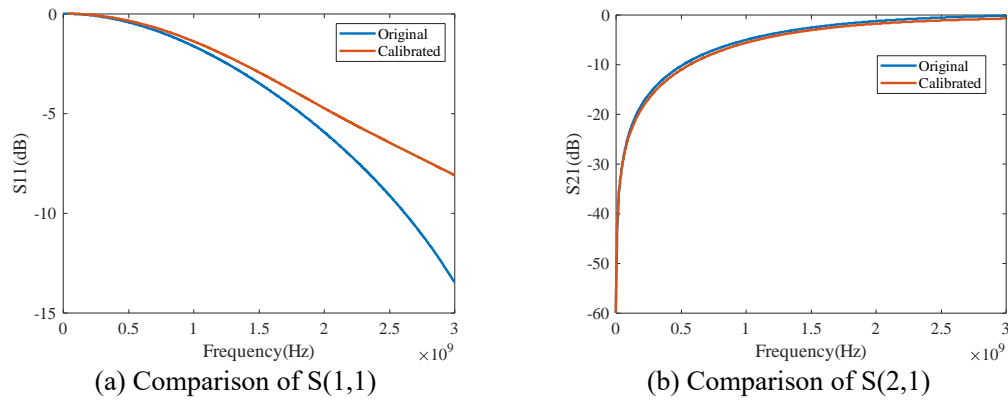


Fig. 31 The comparison between original and calibrated result of $C=1e-12$ F

The remained simulation targets are now completed in the circuit simulator. The data are imported and plotted by MATLAB.

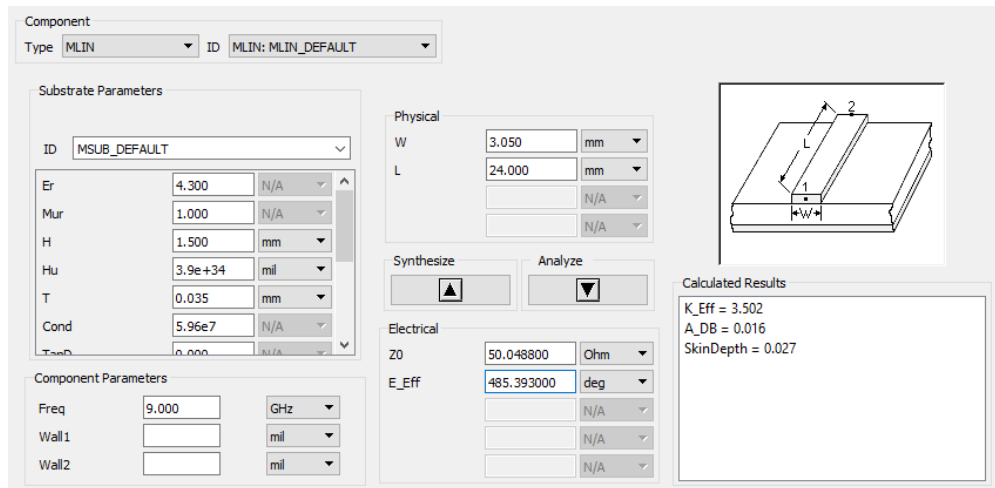


Fig. 32 Calculation of characteristic impedance in circuit simulator

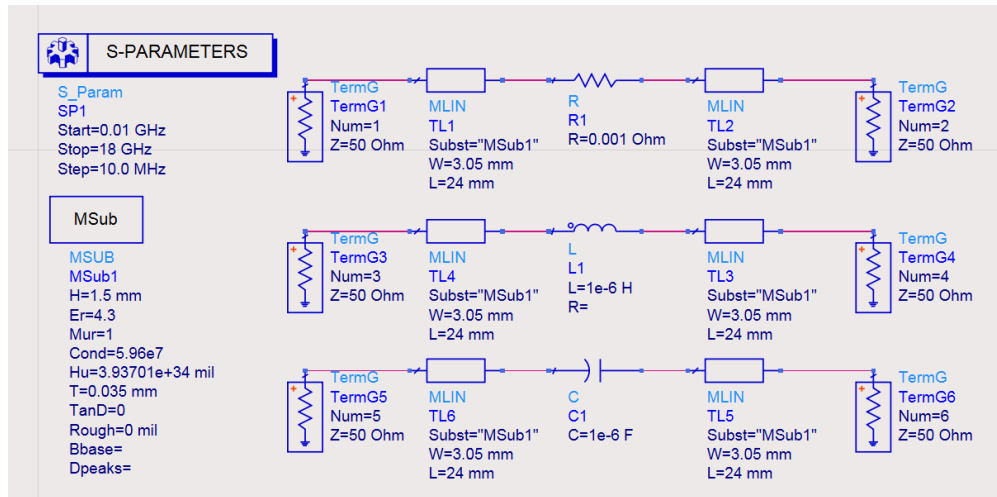


Fig. 33 Schematic of R/L/C element simulation in circuit simulator

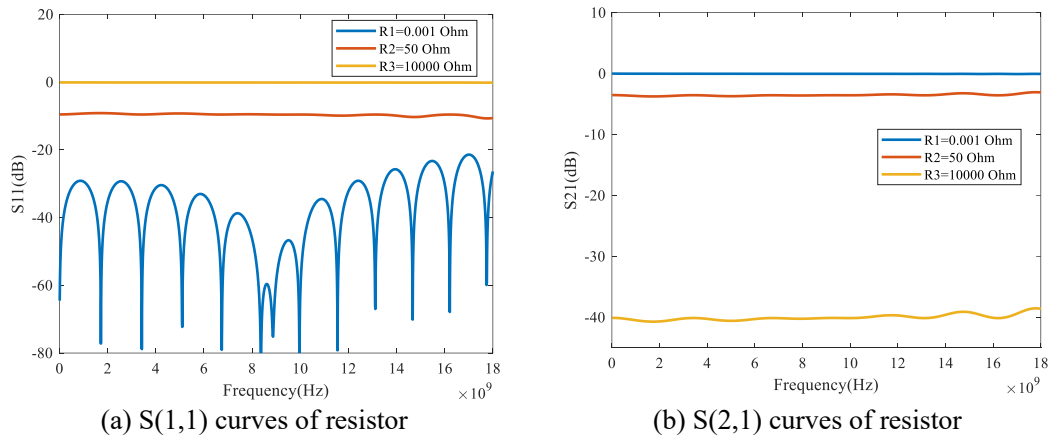


Fig. 34 Comparison of element R

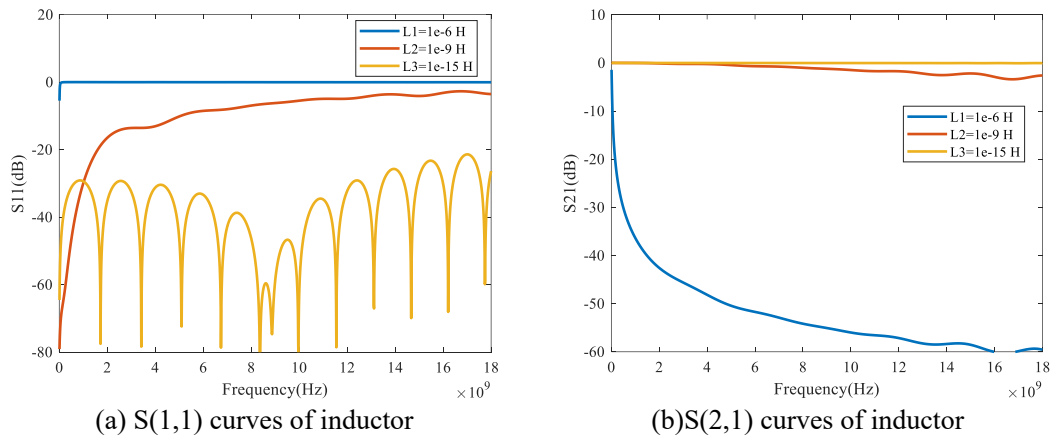
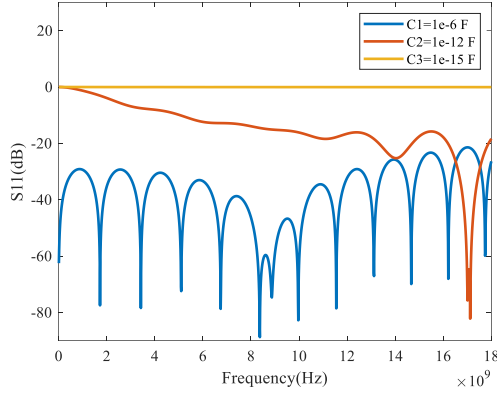
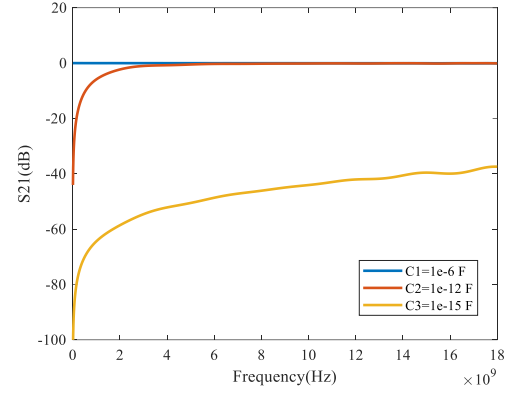


Fig. 35 Comparison of element L



(a) S(1,1) curves of capacitor

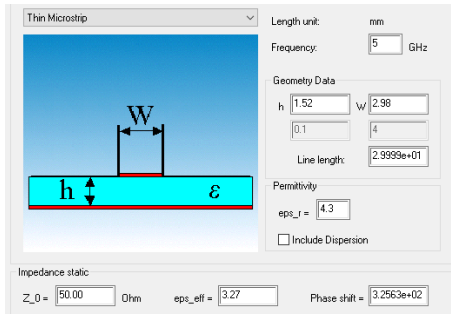


(b) S(2,1) curves of capacitor

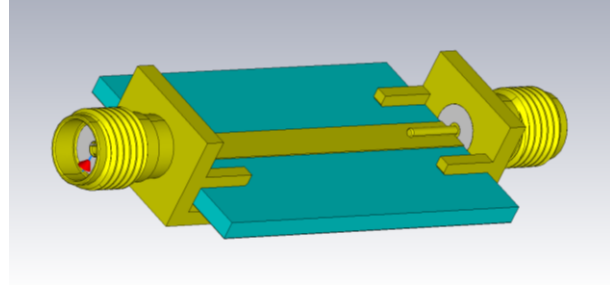
Fig. 36 Comparison of element C

3.2.3 Three-Dimension Model Optimization

In this section, the model of pre-processing transmission model is simulated. Before collecting dielectric, connector and the manufacture of microstrip line on PCB, the model is established and simulated in FIT. The original 3D connector model is established according to the real model, the dimension is shown on the website[24]. The substrate height is 1.52mm, the trace width is 2.98mm. The model is shown in Fig. 37.

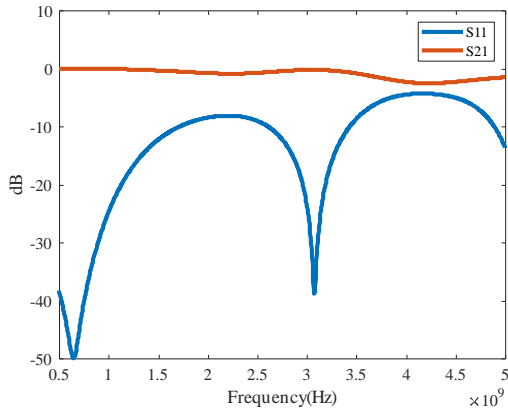


(a) Cross section parameters

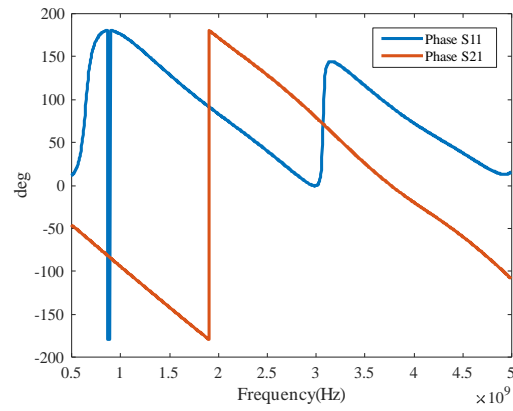


(b) Model of 3D transmission line in FIT

Fig. 37 Simulation model of microstrip line on PCB



(a) Magnitude of S(1,1) and S(2,1)



(b) Phase of S(1,1) and S(2,1)

Fig. 38 S-parameters of simulation for full-wave microstrip line

The frequency range is 500MHz~5GHz, boundary condition is 'open add space', material of dielectric is FR-4 (loss free), relative permittivity is 4.3. Material of line and connector is 'copper(PEC)', the inner core of connector is 'vacuum'. The length of line is 30mm, the height is 1mm, width is 2.98mm and the height of PCB is 1.52mm as shown in Fig. 37(a).

It is obvious that the reflect coefficient $S(2,1)$ is about -4dB around frequency 4~4.5GHz. So the simulation still needs to be improved. For smoothly transmission from coaxial to PCB, we can create a blend at the corner to decrease the distance between transmission line and the outer core as shown in Fig. 39. The angle is 30 degree, the length of the diagonal side of the obtuse angle is 0.3mm.

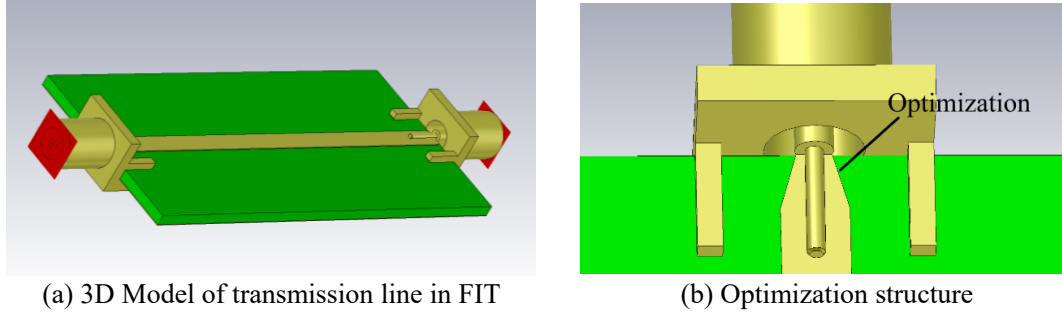


Fig. 39 Simulation model of coaxial to microstrip line

Here we create two microstrip lines, one for 'Thru' model and the length is 50mm, another is for 'Line' model and the length is 60mm. The frequency range is from 10MHz to 18GHz, the result of $S(1,1)$ and $S(2,1)$ is shown in Fig. 40.

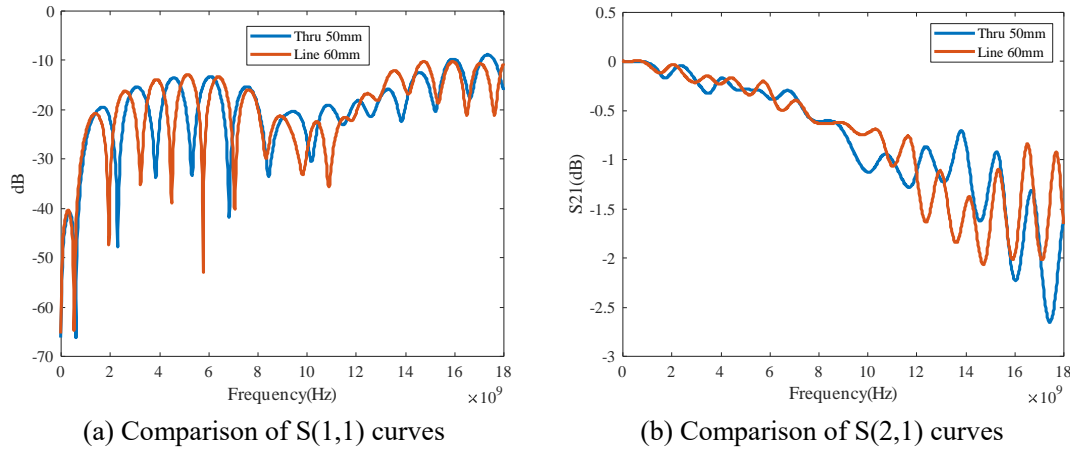


Fig. 40 Comparison between S-parameters of microstrip line for 'thru' and 'line'

The result is more better than before and reasonable, up to 18GHz the transmission coefficient $S(2,1)$ only decreases to -2.6dB.

We can also cut off some ground to try to optimize the simulation result, here sweeping simulation is used and the cut-off rectangular is parameterized by x and z . Two sweeping simulation according to parameters x and z respectively are taken. The definition of x and z is shown in Fig. 41.

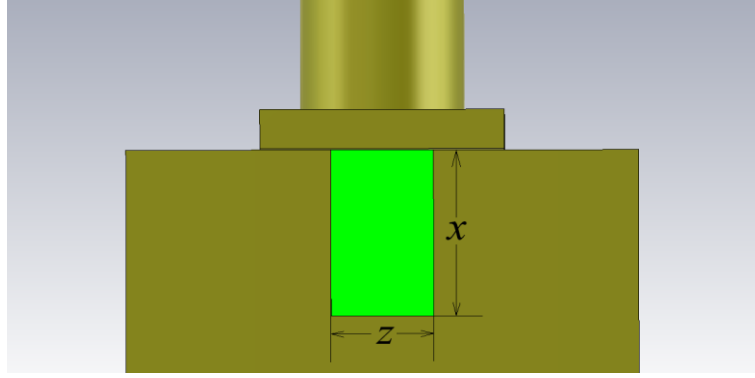
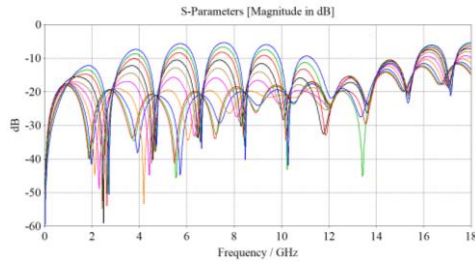
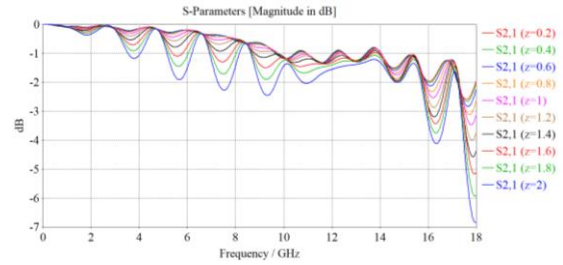


Fig. 41 Top view of the bottom of PCB board for sweeping parameters x and z

The parameterized simulation of z and x are shown in Fig. 42 and Fig. 43 respectively.

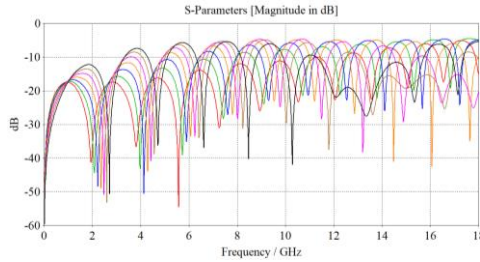


(a) Sweeping simulation results of $S(1,1)$

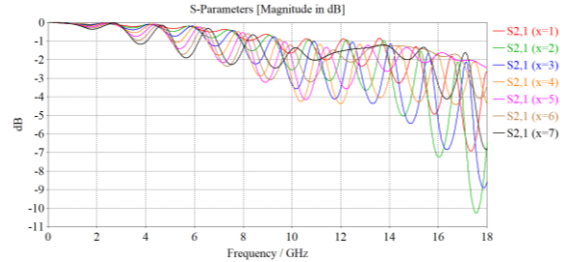


(b) Sweeping simulation results of $S(2,1)$

Fig. 42 Parameterized sweeping simulation of z



(a) Sweeping simulation results of $S(1,1)$



(b) Sweeping simulation results of $S(2,1)$

Fig. 43 Parameterized sweeping simulation of x

In the results of parameterized simulation, the best result is chosen and extracted to compare with the original result as shown in Fig. 44. Unfortunately the result after ground cutting-off is similar and not better than the original one, they are all not satisfied. The optimization still needs to be improved in another way.

Then circuit simulator is utilized to help observe the S-parameters of transmission lines in different situations for different characteristic impedance, the first is 50Ω - 50Ω - 50Ω serial, the second is 50Ω - 55Ω - 50Ω serial. The schematic in circuit simulator software is shown in Fig. 45.

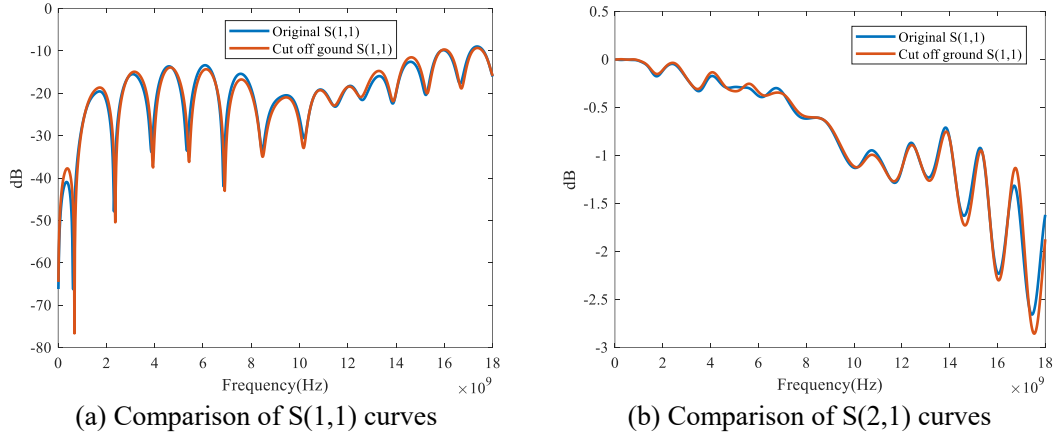


Fig. 44 Comparison with sweeping simulation and original simulation

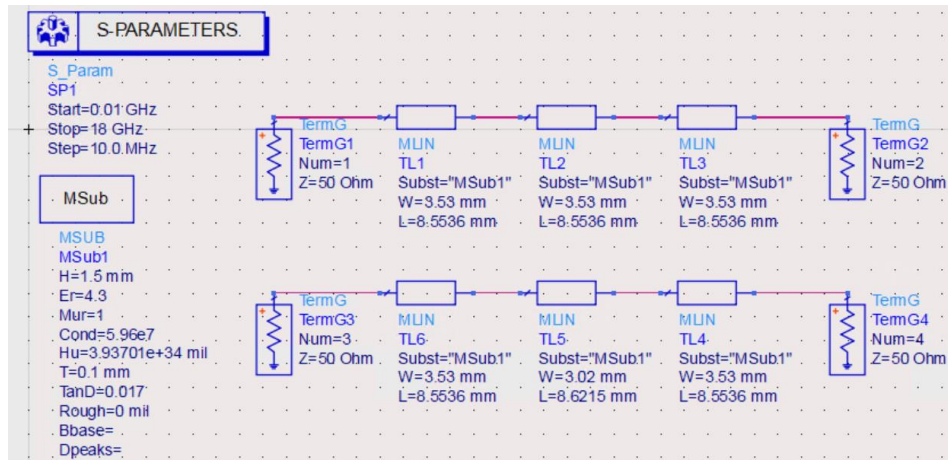


Fig. 45 Schematic of different characteristic impedance serial in circuit simulator

In Fig. 46 the red line stands for the 50Ω-50Ω-50Ω serial transmission line and the blue line stands for the 50Ω-55Ω-50Ω serial transmission line. It is obvious that the reflection coefficient S(1,1) in blue line is higher because of the mismatched characteristic impedance.

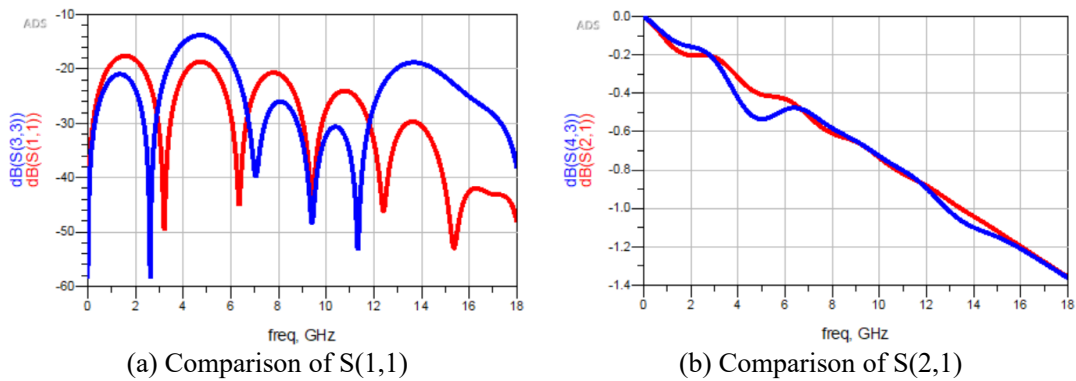


Fig. 46 Comparison of S-parameters for two serial transmission lines
(Red line: 50Ω-50Ω-50Ω; Blue line: 50Ω-55Ω-50Ω)

Then we implement the TDR (Time Domain Reflectometry) simulation to the model to check the reflection

of the whole system[25]. First we adjust the signal to 4ns with a step at 0.25ns and hold on for 3.75ns, the setting and waveform graph is shown in Fig. 47.

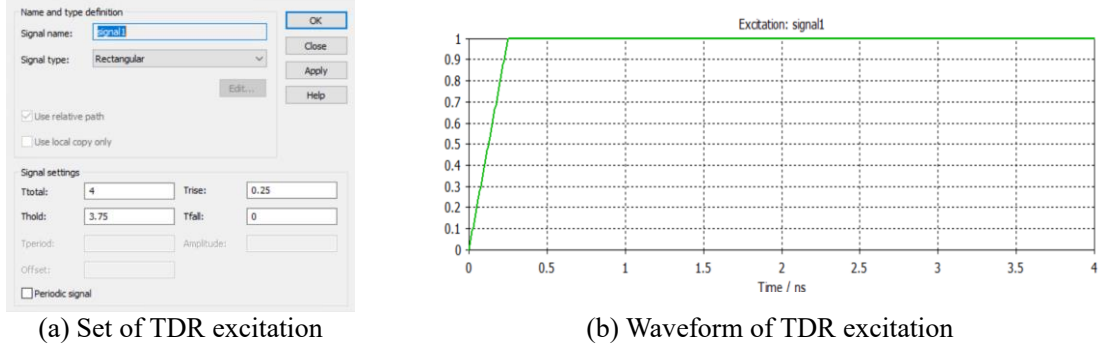


Fig. 47 Setting and waveform graph of step signal

Then we apply two situations into the simulation, as shown in Fig. 48. The red line stands for the model with cutting-off ground ($x=5\text{mm}$, $z=2\text{mm}$), the green dash line stands for the situation without cutting-off ground.

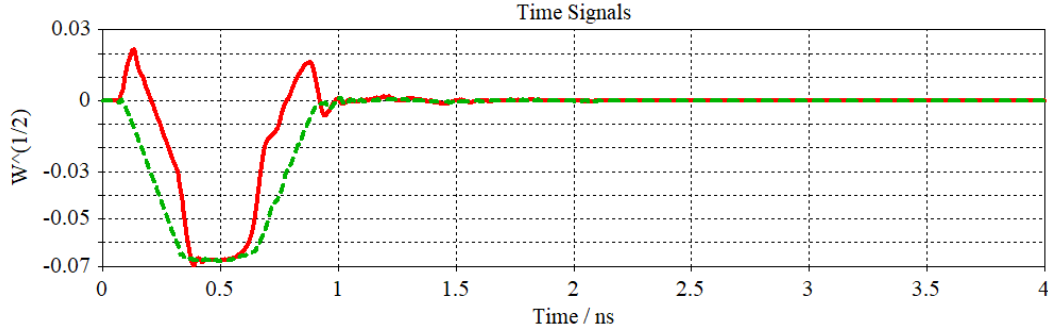


Fig. 48 Reflect signals of two different systems
(Red solid: cutting-off ground; Green dash: no cutting-off)

From Fig. 48 we can easily find that the cutting-off ground will cause a mismatched characteristic impedance, without cutting off the mismatched characteristic impedance will disappear. In Fig. 49, a manual sweeping simulation is operated according to the changing of transmission line tracewidth in order to find the matched characteristic impedance.

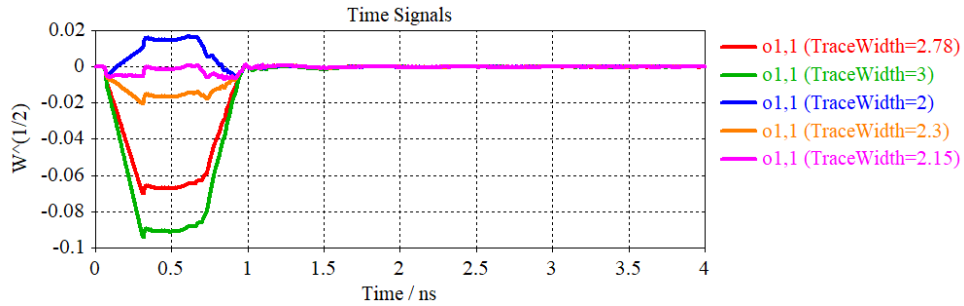


Fig. 49 Sweeping simulation results of TDR

As the pink line in Fig. 49, we adjust the tracewidth to 2.15mm in the simulation to compare with the original 2.78mm tracewidth. Although according to calculation of thick microstrip line if tracewidth is equal to 2.15mm, the characteristic impedance will be 57.45Ω as shown in Fig. 50.

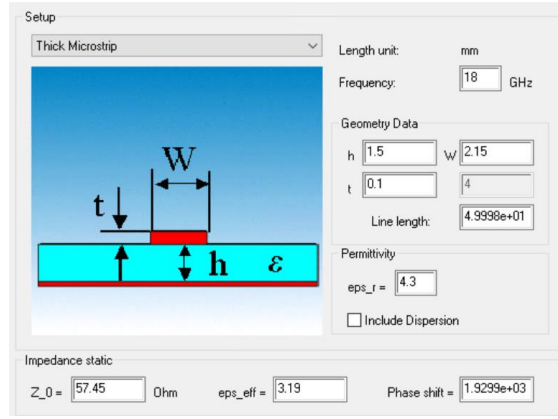


Fig. 50 Impedance calculation in FIT method

The comparison result is shown in Fig. 51. After the adjustment the reflection coefficient $S(1,1)$ is still upon -20dB in the frequency range 8~14GHz.

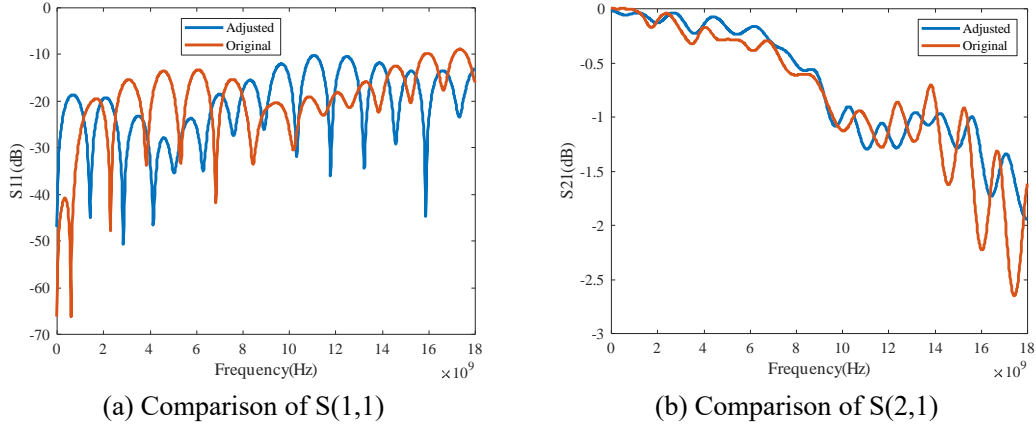


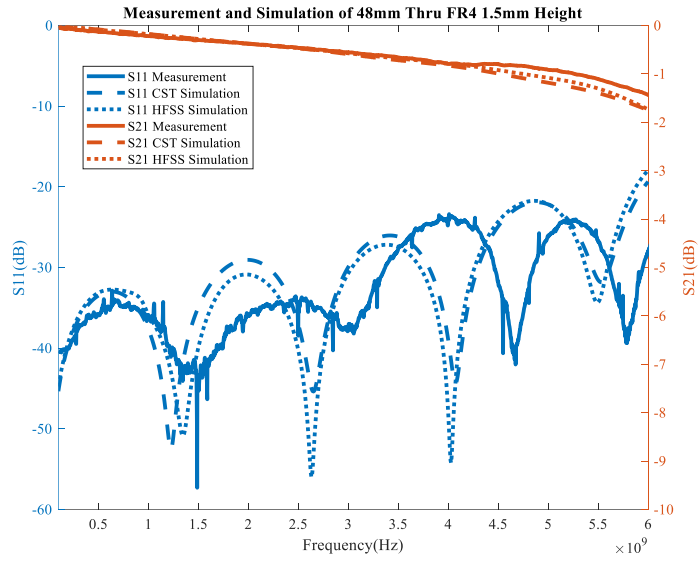
Fig. 51 Comparison of S-parameters between adjusted and original model

3.3 Measurement

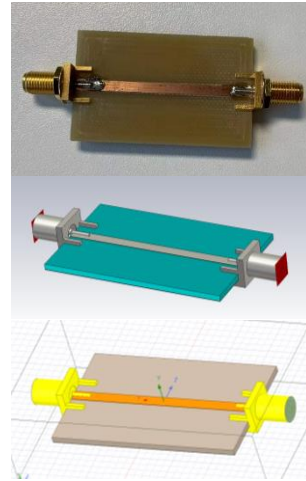
Before measurement, the testing device, so called VNA(Vector Network Analyzer), should be calibrated. In this project, the measurement is completed by the Agilent VNA E8364C, 'SOLT' mechanical method is used for calibration. The calibrated frequency range must cover the range that the experiment needs for measurement.

3.3.1 Comparison

For the measurement of first calibration kits, the frequency range is set up to 6GHz. Measurement, simulation by FIT method and the simulation by FEM are all completed, the boundary condition of FEM method should be set PML(Perfectly Matched Layer)[27]. Now the result of 1st-round measurement is responsible from 100MHz~6GHz as shown in Fig. 52~Fig. 54.

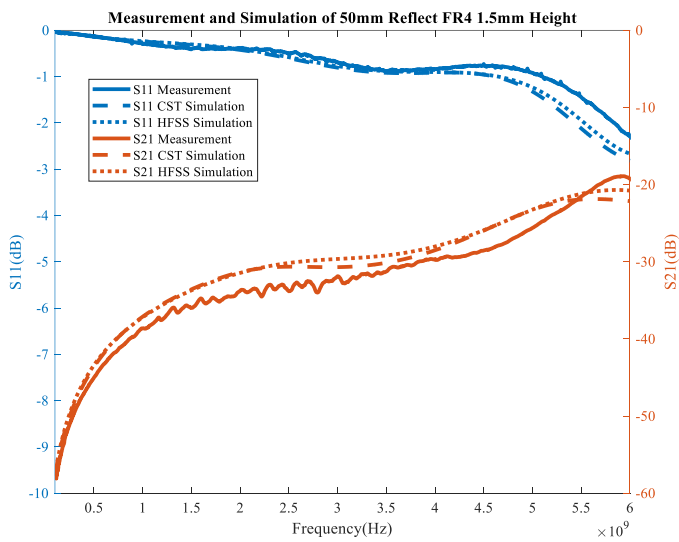


(a) Simulation and measurement of S(1,1) and S(2,1) of 'Thru'

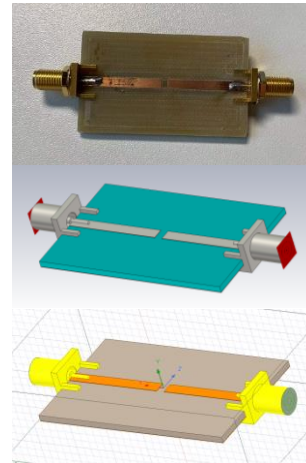


(b) Real and simulation Models

Fig. 52 S-parameter and model of 'Thru'

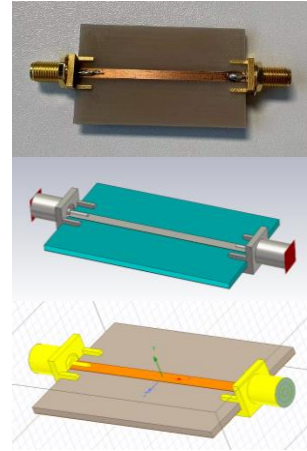
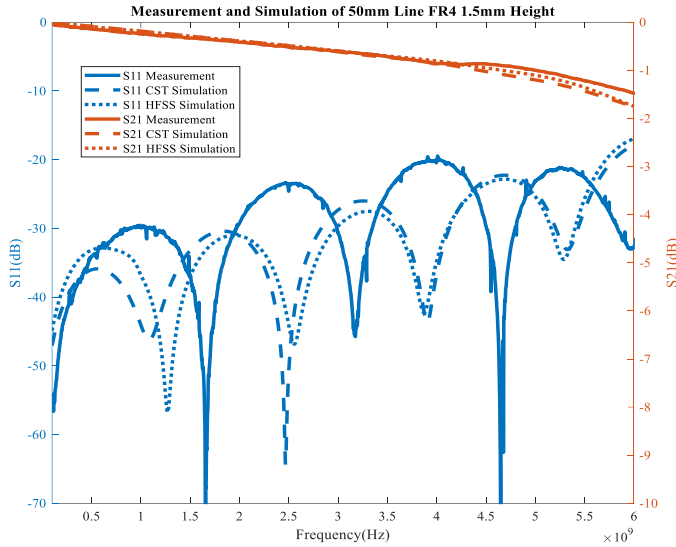


(a) Simulation and measurement of S(1,1) and S(2,1) of 'Reflect'



(b) Real and simulation Models

Fig. 53 S-parameter and model of 'Reflect'



(a) Simulation and measurement of S(1,1) and S(2,1) of 'Line' (b) Real and simulation Models

Fig. 54 S-parameter and model of 'Line'

The results of 'Thru', 'Reflect' and 'Line' from Time-domain simulation, Frequency-domain simulation and measurement are compared. The results are reliable but the phase of measurement differs a lot from the simulation, that is maybe because the permittivity of SMA connector is not accurate, thus the phase is affected.

3.3.2 Optimization

The transition of coaxial line to microstrip line will generate unexpected electromagnetic field, which degrades the transition efficiency of the system[28]. But for coaxial-to-microstrip transition at high frequency, even tiny structures can cause resonances, so the SMA connector should be adjusted[29]. The other structures which as be used to reduce the resonance can be added in the transmission line[30]. Early in last century, the optimization of coaxial-microstrip has been discussed. Chamfers have been created on the protruding pin of coaxial to optimize transmission as shown in Fig. 55(a), a via is also used to make the transition better[31]. In Fig. 55(b), Eric S. Li makes some adjustments in geometry and implements vias in the PCB board to improve the coaxial-microstrip transition[32]. Later as shown in Fig. 55(c), to avoid the cumbersome manufacture process of PCB, the author optimizes the geometry of SMA adaptor in another way[33].

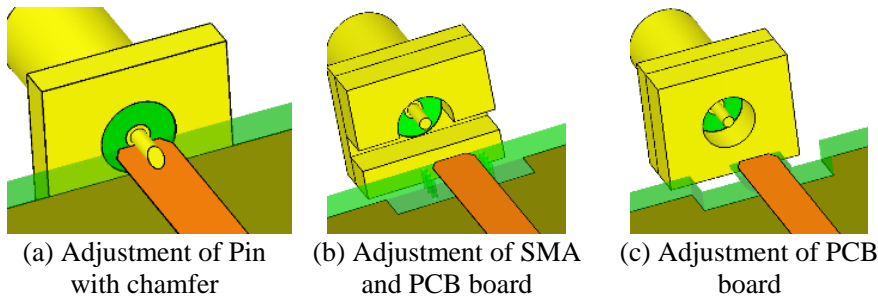
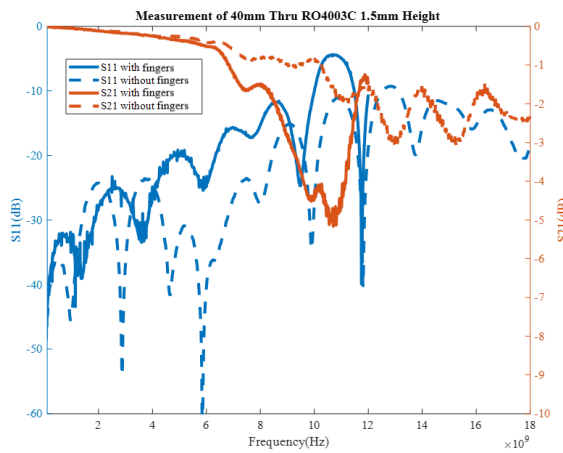


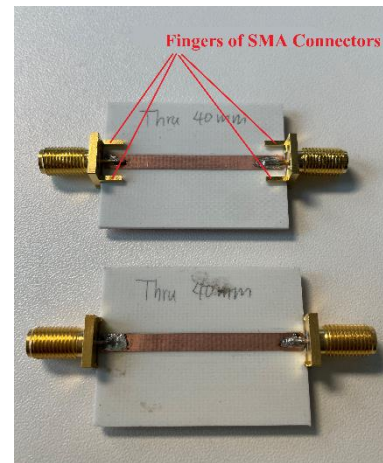
Fig. 55. Schematics of existing optimization about coaxial-microstrip

In the initial simulation of 3D SMA-Microstrip model, there will be an obvious resonance around frequency 10~12GHz the resonance is mainly caused by the upper two fingers of the SMA. In order to deal with that, the SMA manufacturer provides a suggestion of SMA pad and the drilling hole used for eliminating the resonance frequency cause by the upper two fingers. Due to the constraints of the manufacturing conditions, the vias cannot be easily processed. To remove the resonance frequency caused by this kind of SMA adaptor, the upper two fingers are simply cut off so that only the lower two fingers and the pin need to be soldered to the microstrip line.

For higher frequency implementation, the VNA is operated by mechanical calibration method 'SOLT' up to 18GHz. Through measurement we find that there is a resonance around 11GHz, we suspect that there is a resonance frequency caused by the two fingers of the SMA connector, so the fingers are cut off and results are compared. As shown in Fig. 56, the measurement of S-parameters for with fingers uncut and fingers cut off based on the 40mm 'thru' microstrip line RO4003C substrate height 1.5mm. The result shows that the S-parameters will be better if the fingers are cut off.

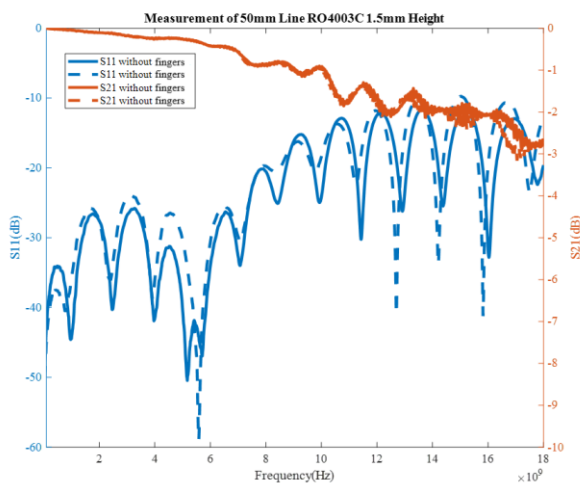


(a) S11 and S21 comparison

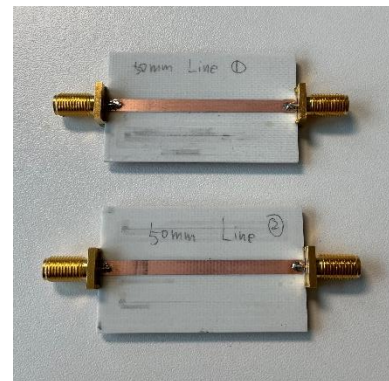


(b) Models

Fig. 56 The measurement result with and without the fingers of SMA connector



(a) S11 and S21 comparison

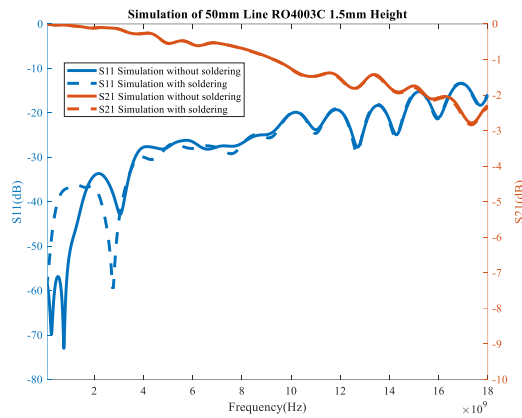


(b) Models

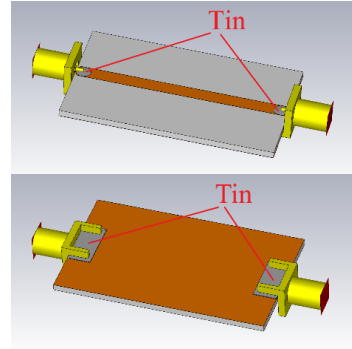
Fig. 57 Comparison of the two 'Line' models

For comparison with the same model produced nearly at the same time, to observe the consistency of our fabrication, we manufactured two 50mm 'Line' models and get them measured, the result is shown in Fig. 57. Summary: The trend of S-parameters are similar, but there is still some difference between the two results, it is mainly due to the fabrication accuracy, we may investigate the range and reason of the difference deeply in the future.

The models in simulation do not contain the modeling of soldering (material Tin). The result is shown in Fig. 58. It shows that at high frequency, the S-parameter of with and without Tin soldering is almost the same.

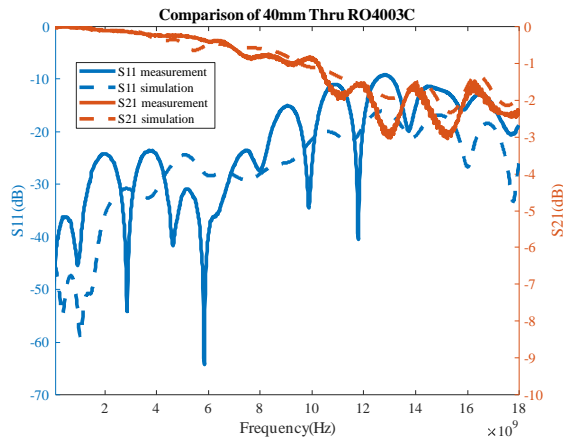


(a) S11 and S21 comparison

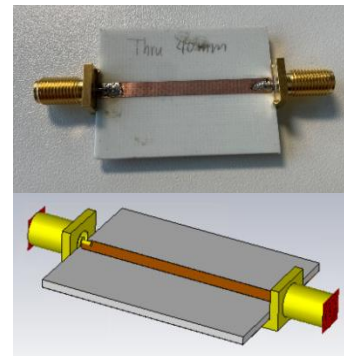


(b) Model with soldering

Fig. 58 Comparison of simulation with soldering modeling and without soldering modeling

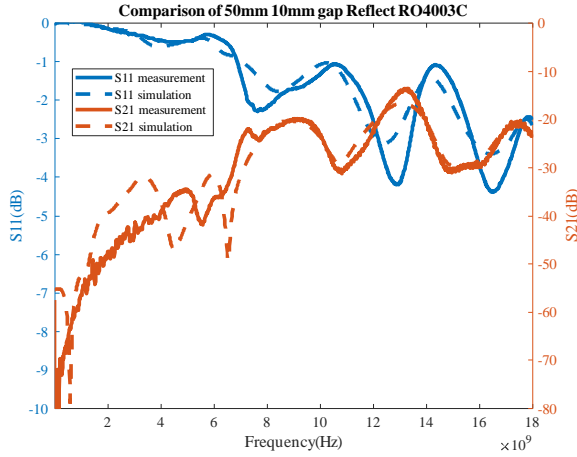


(a) Comparison of measurement and simulation

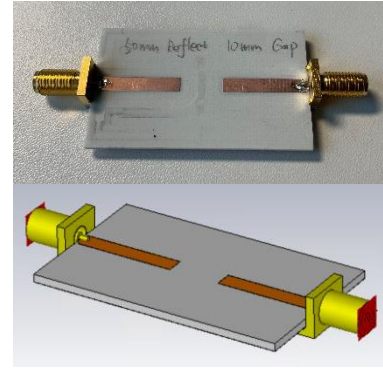


(b) Real and simulation models

Fig. 59 Comparison of measurement and simulation of 40mm 'Thru' (Material RO4003C)

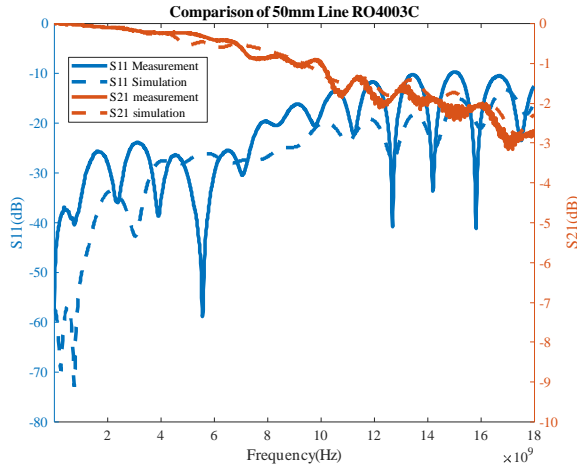


(a) Comparison of measurement and simulation

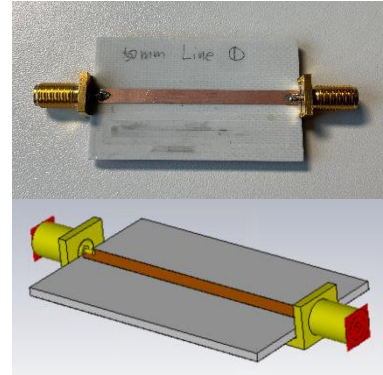


(b) Real and simulation models

Fig. 60 Comparison of measurement and simulation of 50mm 'Reflect' (Material RO4003C)



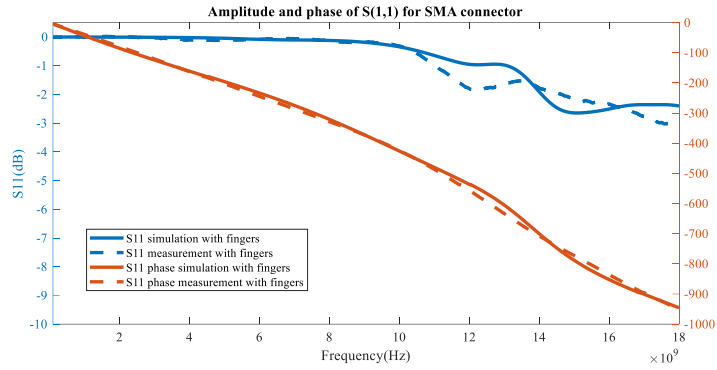
(a) Comparison of measurement and simulation



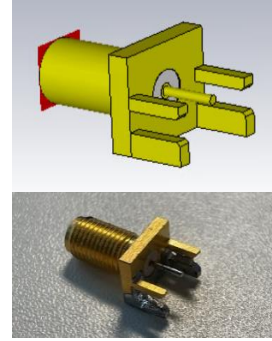
(b) Real and simulation models

Fig. 61 Comparison of measurement and simulation of 50mm 'Line' (Material RO4003C)

Then we established the models as the measured geometric parameters and did simulation in FIT method software, and also measured the $S(1,1)$ of the SMA for three situations such as 'with fingers', 'without two fingers' and 'without any fingers'. If the relative permittivity of the dielectric is set to 1.9, the phase of $S(1,1)$ will have a good consistency up to 18GHz as shown in Fig. 62 ~ Fig. 64.

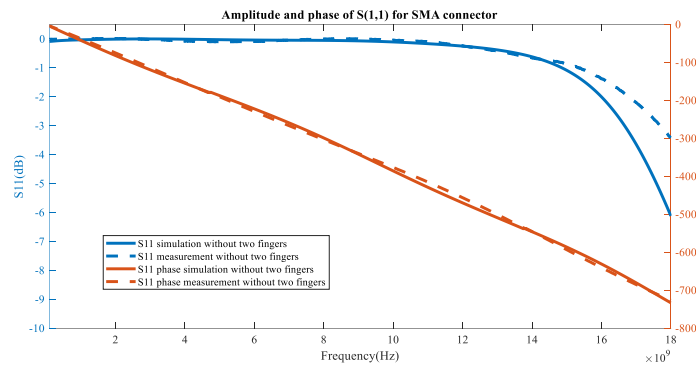


(a) S(1,1) and the phase of simulation and measurement

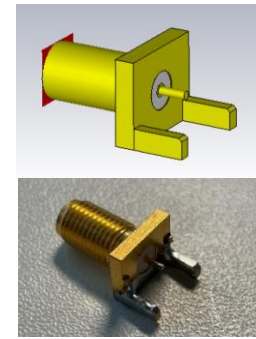


(b) Model and Real object

Fig. 62 Simulation and measurement of SMA with fingers

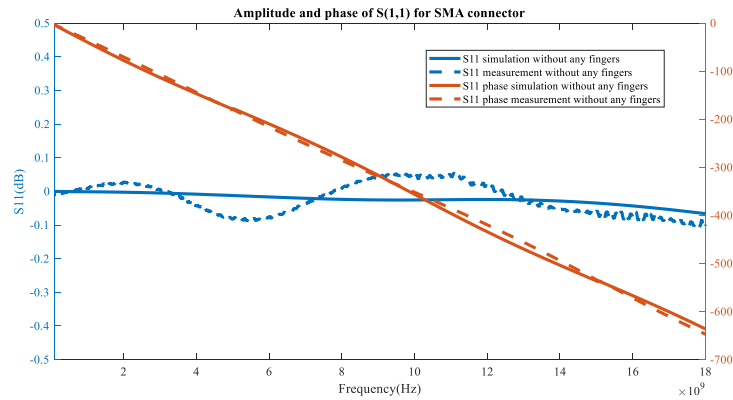


(a) S(1,1) and the phase of simulation and measurement

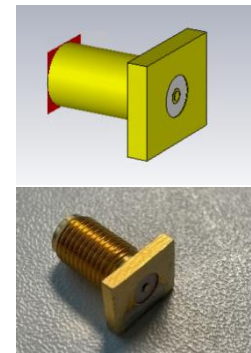


(b) Model and Real object

Fig. 63 Simulation and measurement of SMA without two fingers



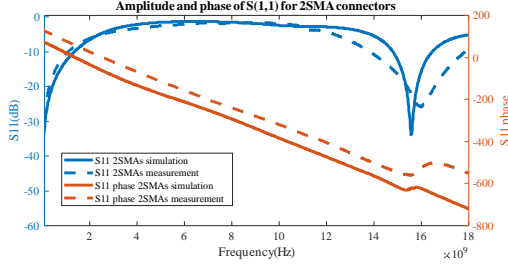
(a) S(1,1) and the phase of simulation and measurement



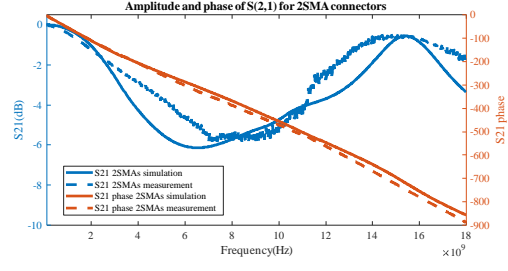
(b) Model and Real object

Fig. 64 Simulation and measurement of SMA without any fingers

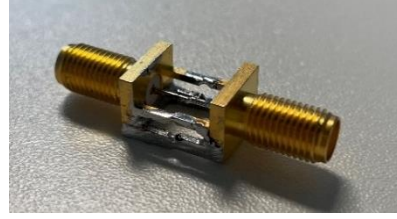
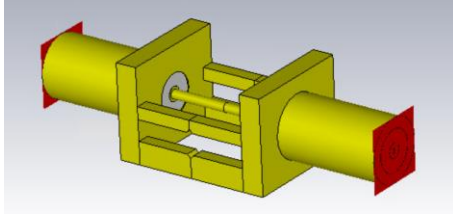
It is obvious that the relative permittivity of Teflon dielectric inside the SMA should set 1.9 instead of vacuum or 2.1 from the official website.



(a) S(1,1) and the phase of simulation and measurement



(b) S(2,1) and the phase of simulation and measurement



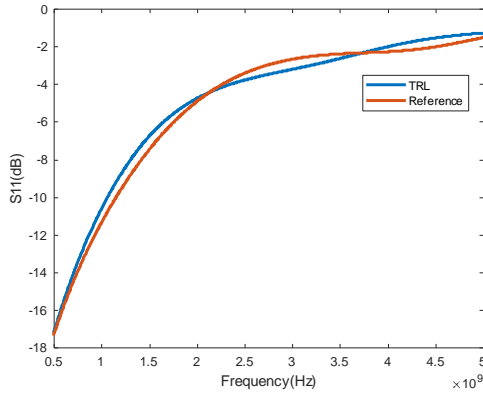
(c) Simulation model (left) and real object (right)

Fig. 65 Simulation and measurement of two connected SMA connectors

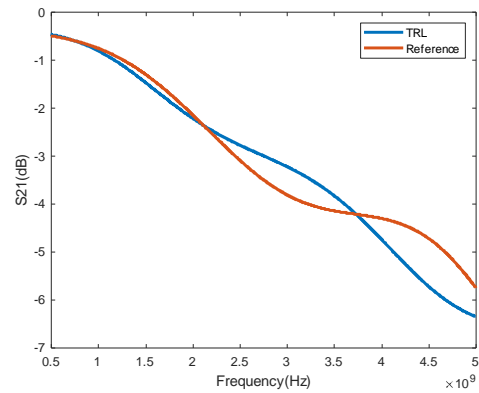
We use two SMA connectors connecting directly to measure the S-parameters to verify the right relative permittivity, the result is shown in Fig. 65. That proves the updated permittivity is accurate.

3.4 Verification

Now before the complement of measurement, in order to make sure the TRL calibration is reliable, we have to simulate and implement the TRL calibration at first. The length of 'Thru' is 48mm, gap of 'Reflect' is 2mm, length of 'Line' is 50mm, the 'R/L/C' device under test will be 5Ω , 5nH and 5nF respectively. The reference result is obtained by simulation that the DUT is directly touched by the excitation without any transmission line as the condition in section 3.2.2.



(a) Comparison of S(1,1) curves



(b) Comparison of S(2,1) curves

Fig. 66 Comparison of TRL and reference S-parameter for DUT= 5Ω

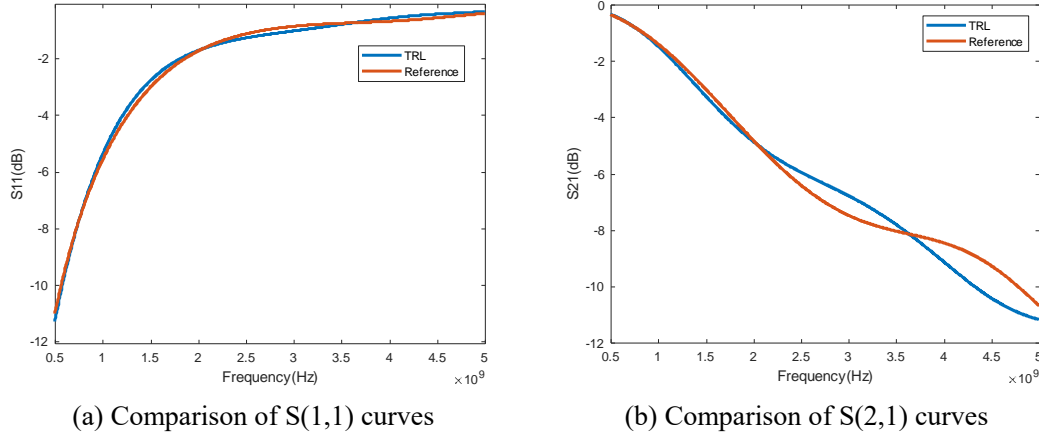


Fig. 67 Comparison of TRL and reference S-parameter for DUT=5nH

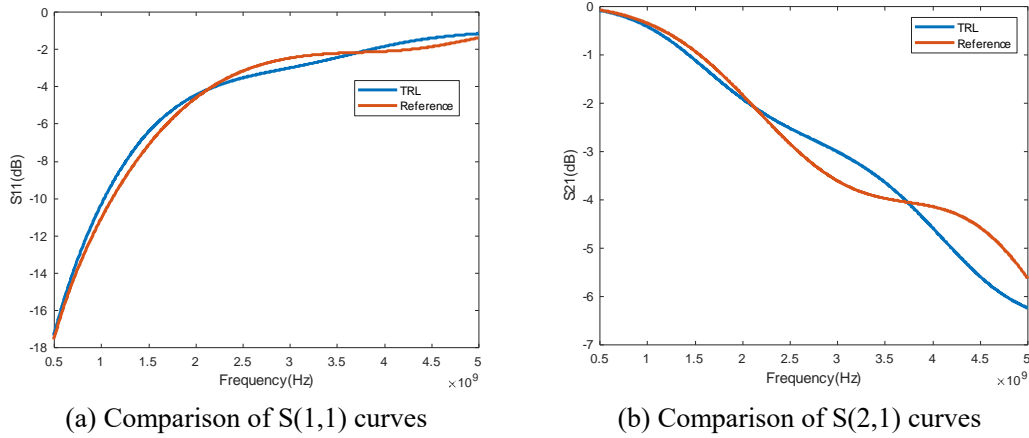


Fig. 68 Comparison of TRL and reference S-parameter for DUT=5nF

The result of TRL calibration based on simulation data shows that the TRL calibration result is reliable, thus it is possible for us to go deeper into TRL calibration of reality measurement data. The TRL calibration code is provided by Michael Wulff.

3.5 Summary

This section shows the main job of the research project, the TRL calibration method is verified, the calibration kits are completed, optimization aiming at improving the reliability of calibration is processed, and the measurement is done. The part of de-embedding process in the original proposal is investigated in this section.

1. Due to the degradation of equipment performance. Before measurement, it is important to judge whether the VNA is in a good condition or not. There are too many glitches in the curve, which means the VNA is no in a good condition, so this VNA can hardly satisfy the high frequency research.
2. In order to achieve a good consistency between simulation and measurement. Every aspect such as permittivity, geometry, VNA calibration should be checked. The parameter provided by company or manufacture may not be accurate. In this section, the results of 'Thru', 'Reflect' and 'Line' from Time-domain simulation, Frequency-domain simulation and measurement are compared. The results are reliable but the phase of measurement differs a lot from the simulation, that is because the permittivity of SMA connector is not accurate, thus the phase is affected. So the SMA connector is modelled and verified by simulation and experiment, thus the permittivity is adjusted.

3. In the high-frequency application range of centimeter or millimeter waves, tiny structures will cause resonance. Therefore, in the investigation, the structure of products can be adjusted to a certain extent to meet the actual situation in the project, for example to eliminate the resonance.
4. An important condition for determining the quality of a transmission line is whether the characteristic impedance is consistent. The TDR method and TDR machine can easily observe the characteristic impedance matching of the transmission line to help adjust the structural size of the transmission line.

4 De-embedding of 3D Element Package

In previous chapters, TRL calibration is discussed, verified and implemented as a de-embedding method. Through TRL calibration we can obtain the S -parameter of 3D device packages, pads, and a short transmission line included.

But even elements with the same parameter will be utilized in many different application conditions, such as different transmission line widths, different pads, different PCB substrate heights, PCB materials with different dielectric permittivity, and even embedded in different package. Just like the model synthesis mentioned in the original research proposal. In this section, we will use the hybrid method including simulation and measurement to further strip away the interference such as pad, packaging contained in the DUT parameters obtained by TRL calibration, and obtain the intrinsic parameters of the element, which can be accurately generalized to any other application situation[34][35]. It will be verified in this section, this method is highly dependent on the consistency of simulation and measurement.

For the fixture with DUT implemented in this article, it can be analyzed through Fig. 69, where D represents the scattering matrices of the element. Specifically, the short transmission line, pad, package are all included in matrix S . More detail process is shown in Fig. 73.

The fixture is represented by a general 3-port network, no assumptions are made about its electrical characteristics, the first 2 ports of the network are the external ports of the fixture, which are connected to the measuring instrument, and the other one-port is the port of the device. So the S matrix can be processed as[36][37]:

$$S = \begin{bmatrix} S_{2 \times 2} & S_{2 \times 1} \\ S_{1 \times 2} & S_{1 \times 1} \end{bmatrix} \quad (4-1)$$

When the DUT is embedded in the fixture, the total scattering matrix measurement S_M can be expressed as:

$$S_M = S_{2 \times 2} - S_{1 \times 2} (S_{1 \times 1} - D^{-1})^{-1} S_{1 \times 2} \quad (4-2)$$

Solving this equation, the D matrix is expressed as:

$$D = \left[S_{1 \times 1} - \left[S_{2 \times 1}^{\dagger} (S_{2 \times 2} - S_M) S_{1 \times 2}^{\dagger} \right]^{-1} \right]^{-1} \quad (4-3)$$

where \dagger stands for the Moore-Penrose generalized inverse.

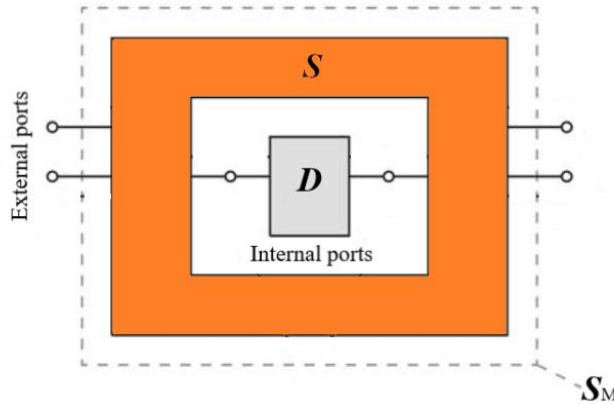


Fig. 69. Schematic of DUT embedded with a fixture

The de-embedding method can be used directly without TRL calibration, but the accuracy of this method depends a lot on the consistency between simulation and measurement. With TRL calibration we can at least eliminate the mismatch caused by the conversion of coaxial-PCB, thus the consistency between measurement and simulation can be further guaranteed.

4.1 Simulation Verification

For a normal result of simulation for a transmission line, the calculation of matrix D should be accurate and the verification should be reliable. In this section, a 50mm transmission line with a 4.7pF capacitor is verified in FIT method.

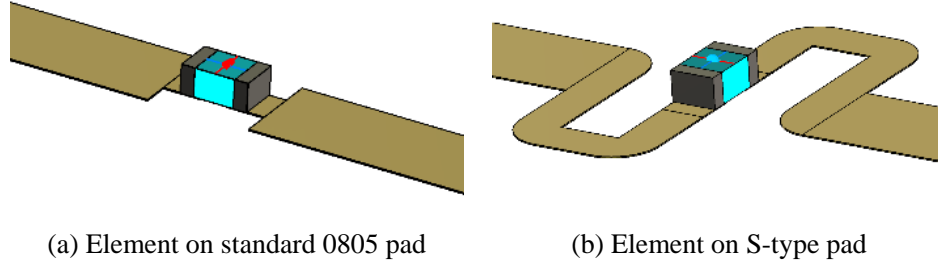


Fig. 70. The simulation package model and the complex implementation S-type pad in FIT method

The S matrix (3×3) can be obtained from the 3-port simulation and the S_M matrix can be obtained from the original 2-port simulation with a 4.7pF capacitor. To deeply verify the reliability of the solution for embedded equation and also to demonstrate the use of the TRL calibration application in solving embedded equations, the matrices S and S_M are replaced by the matrices after TRL calibration, thus the influence of coaxial-PCB transition can be eliminated. After TRL calibration calculation the matrices T_1 and T_2 can be obtained. The S matrix can be obtained by de-embedding the matrices T_1 and T_2 from the original simulation result S' matrix(.s3p).

Thus, the calculation result is verified through Term1-s2p-Term2 and Term1-s3p(s1p)-Term2 simulation in the circuit simulator. From the result in Fig. 71, it is obvious that the two S-parameter results are matched perfectly, that means the right S-parameter of the DUT is obtained. The solution of embedded equation is reasonable.

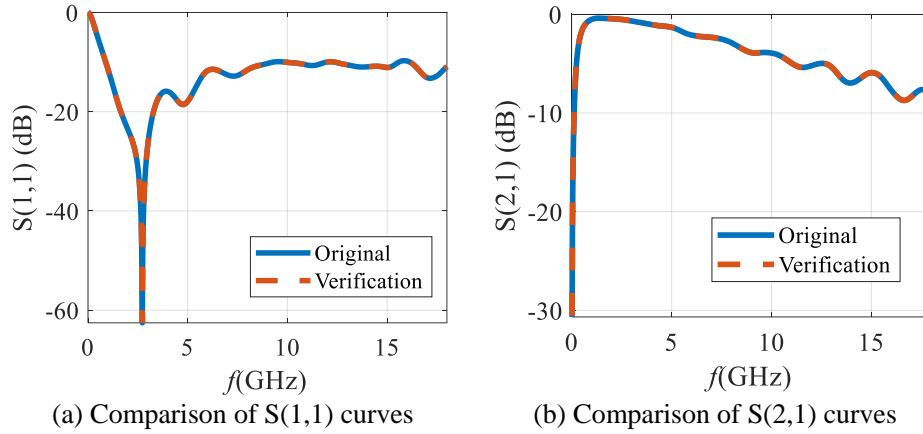


Fig. 71. The verification result of embedded equation in standard 0805 pad implementation

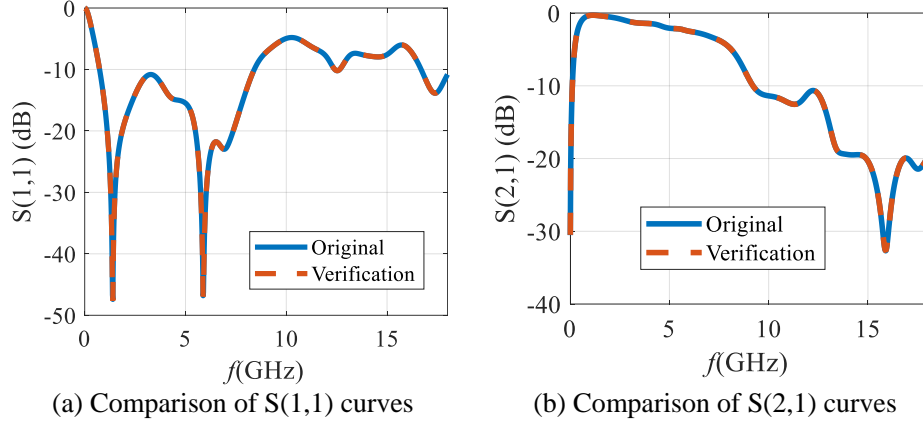


Fig. 72. Further verification result of importing \mathbf{D} matrix into the S-type pad implementation

To deeply verify the reliability of the solution for embedded equation, the pad of capacitor and the material of substrate are changed to RO4003C respectively, and another \mathbf{S} matrix and another \mathbf{S}_M matrix are obtained, but the matrix \mathbf{D} remains. The comparison result is shown in Fig. 72. It is obvious that the two results are very close, which means the de-embedded \mathbf{D} matrix is responsible and can be used universally.

4.2 Experimental Verification

After the verification of the embedded equation. It should be implemented into the de-embedding of real component measurement based on TRL calibration. The flow chart is shown in Fig. 73.

As told in the last subsection, TRL calibration can be used to eliminate the influence and transition inconsistency of coaxial-SMA, and the matrix \mathbf{S}_M is obtained from measurement, while the matrix \mathbf{S} is obtained from simulation, TRL calibration, and two fixtures de-embedding.

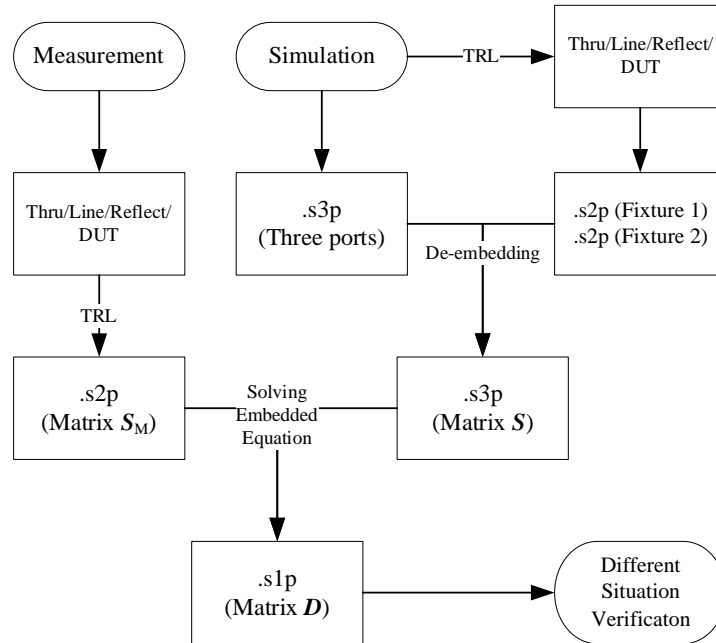


Fig. 73. The solution flow chart of combination of TRL calibration and embedded equation

According to Fig. 73, the S-parameter matrix \mathbf{D} of the device under test is calculated by using the matrix \mathbf{S}_M obtained from the measured data and the three-port matrix \mathbf{S} obtained by simulation. Matrix \mathbf{D} is substituted return into the three-port S-parameter \mathbf{S} matrix for comparison with the original \mathbf{S}_M matrix, as shown in Fig. 74.

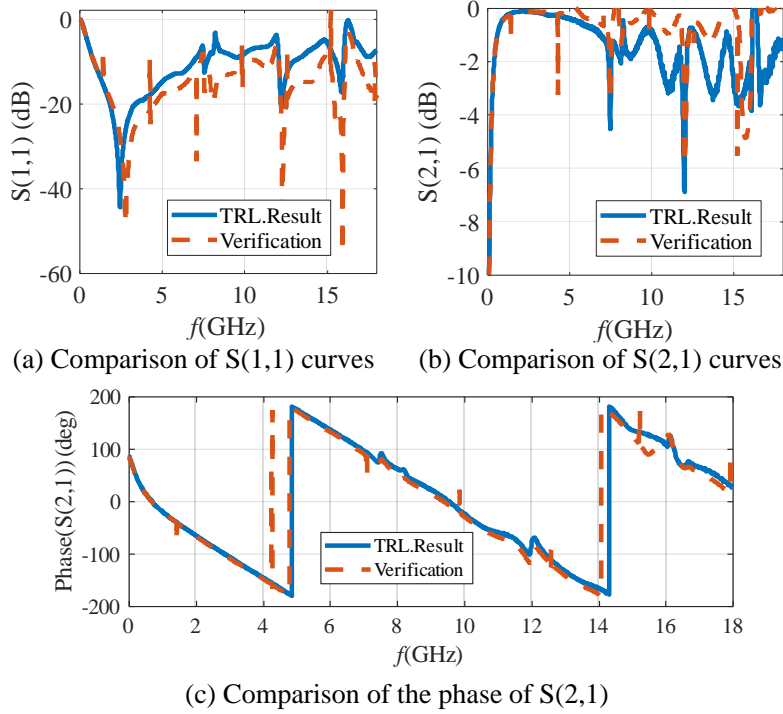


Fig. 74. The measurement verification result of embedded equation in standard 0805 pad implementation

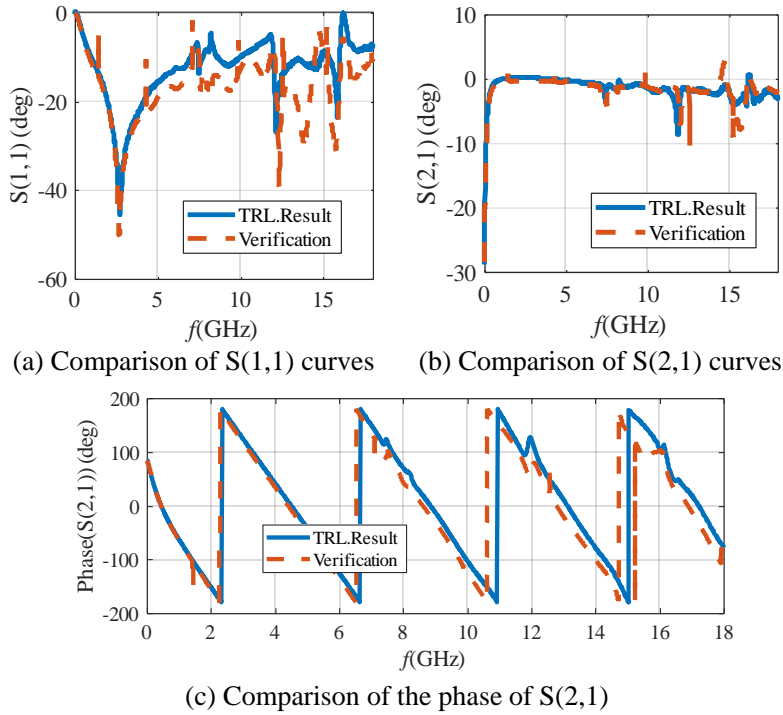


Fig. 75. Further measurement verification result of importing \mathbf{D} matrix into longer launch implementation

For more verification, first the length of DUT is changed, extending for 20mm, then the matrix D calculated remains and is substituted into the new S matrix, the result is show in Fig. 75. Then for further verification in another different implementation, a new calibration fixture is manufactured and the substraight height is reduced to 1mm. After the substitution of D matrix, the result is shown in Fig. 76. Similarly, the same D matrix is substituted into the complex S-type pad implementation and the result is shown in Fig. 77.

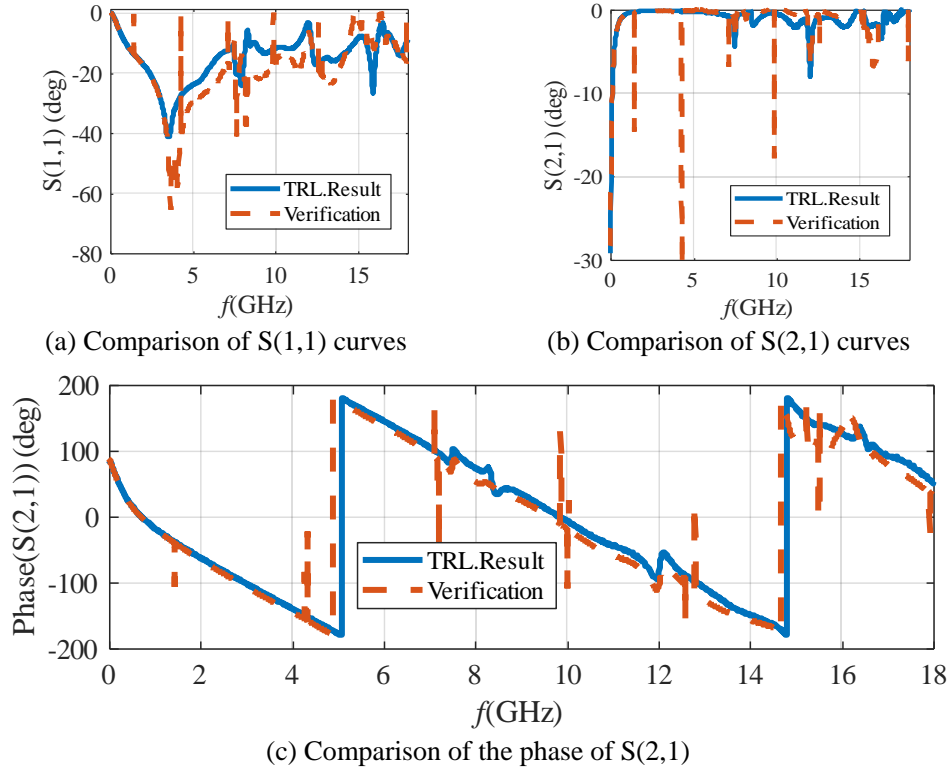


Fig. 76. Further measurement verification result of importing D matrix into thinner launch (1mm) implementation

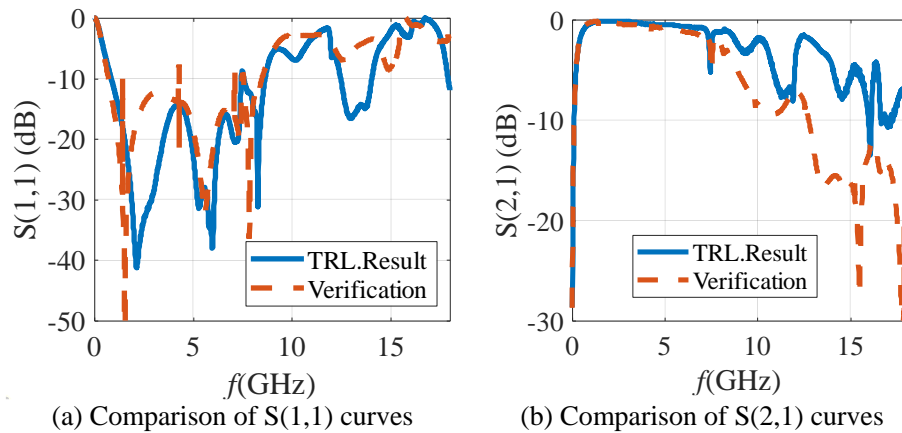


Fig. 77. Further measurement verification result of importing D matrix into the S-type pad implementation

As can be seen from the results above, since the frequency exceeds the range recommended by the DUT manufacturer ($<8.5\text{GHz}$), when the frequency goes higher, the verification result will become worse.

Moreover, since the accuracy of the de-embedding results is highly dependent on the consistency of the measurement and simulation after TRL calibration, when the DUT being calibrated and its implementation pad become more complex, the accuracy of the verified results will also decrease.

4.3 Summary

In the verification of simulation, the extracted parameter of element is accurate and can be implemented successfully in different conditions. That means the de-embedding method composed by simulation and measurement is reliable. The parameter of element extracted is accurate, which means the package, pad can be further de-embedded.

Theoretically, the de-embedding method in this verified in this section is still valid if it is not calibrated by TRL method. The purpose of TRL calibration is to eliminate the influence of coaxial-PCB at both sides of the transmission line, so as to make the results of simulation and measurement as consistent as possible, because this method is a combination of simulation and experiment. It is highly dependent on the consistency of simulation and experimentation.

5 Fabrication Overview

In this report, most of the processing is done independently by the author in the institute. The equipment of the institute is sufficient for the processing of microstrip lines, soldering of SMA connectors, and soldering of DUT.

5.1 Fabrication Method

The overview of the operation on LPKF PCB Prototyping Machine will be shown as following. For the manufactory of the transmission line in this project, we have to use the PCB prototyping machine to produce the microstrip lines we need. The whole processing platform is shown in Fig. 78.



Fig. 78 LPKF processing device and the controlling computer

1. Open the 'CircuitPro PM 2.5' software, complete the connection to 'S63' by the Circuit Pro software, if practicing, connect to 'Virtual'. At this time, the whole PCB board should also be put and stuck on the white board
2. 'New File' – 'Templates' – 'SingleSided_Bottom.cbf' or 'SingleSided_Top.cbf';
3. 'Processing planning wizard', choose the PCB, the style of layer, the material (FR4/RO4003C/RO4350B), then finish.
4. Import data from a non-native format or draw some simple plot in the software, here if the geometry of the microstrip line is simple, we draw the plot directly in the software by creating 'rectangle' based on the 'Start point' and 'End point' of X & Y axis.
5. If the plot is complex, for the accurate processing and convenience, we can import the .dxf document into the 'CircuitPro PM 2.5'. The tips are, first the .dxf document should be created in the HFSS software. If exported from FIT METHOD software, there will be error in importing into 'CircuitPro PM 2.5'. When exporting the model to .dxf document in HFSS, make sure the face to be drawn should be perpendicular to the Z axis. After importing the .dxf document into CircuitPro PM 2.5, the board line and the copper layer should be defined manually.
6. After completing the plot of microstrip line, we should let the machine be aware of the trace it has to proceed – 'Generate isolation and contour routing toolpath';
7. Move the plot to the suitable place, we can shut down the 'Mouse cursor' and use the mouse to control the drill holder's moving;
8. Then check if all the drills are installed, if not, install the drills one by one and set the drill information

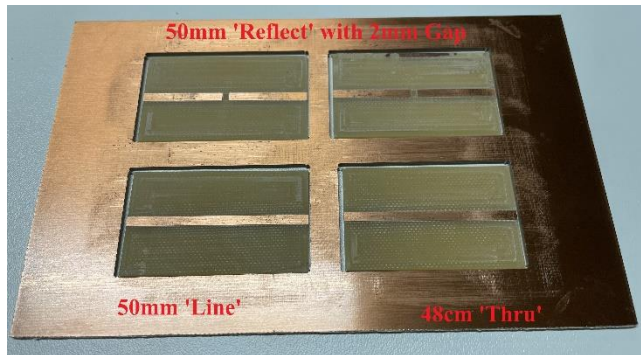
in the software;

9. 'Board production wizard' – start the prototyping;

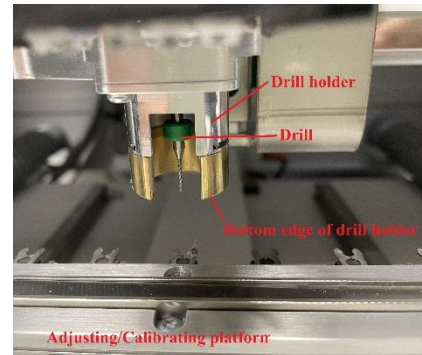
However there are still some problems in the precision of processing.

As shown in Fig. 79(a), the SubstrateHeight of FR4 is 1.5mm, and the thickness of copper is 0.1mm, but if these parameters is set as that in the Circuit Pro software, the copper layer will not be clearly cut off. In fact, we set the thickness of copper 0.12mm, thus the copper layer can be cut off but there is a new problem that the bottom edge of drill holder, shown in Fig. 79(b), will also touch the copper layer of PCB board. As shown in Fig. 79(a), there are a lot of scratches around the outline of microstrip line and also scratches on the trace.

So we suspect that, since the uneven of PCB board or white board, there are some problem in the precision of machining. So we should make a little adjustment, not only changing the setting of copper layer, but also the SubstrateHeight.



(a) A set of processed lines by LPKF





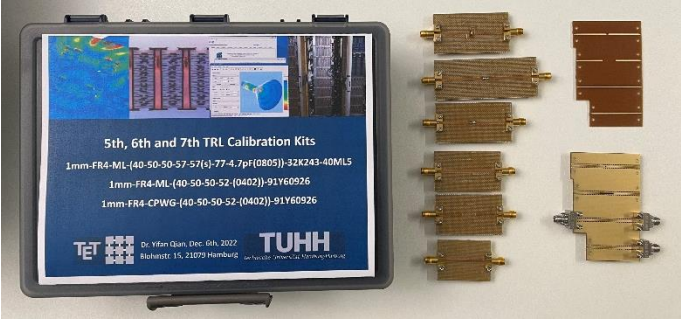
(b) Drill and the holder in the LPKF

Fig. 79 Pictures of processed microstrip line and the drill in LPKF

5.2 Fabricated Calibration Structures

The pictures of calibration kits and transmission lines are all shown in Table 3.

Table 3 Fabrication Overview

No.	Material & Substrateheight	Connector	Type
1st	FR4 1.5mm	Molex-SMA-73251-1290	Microstrip Line
2nd	RO4003C 1.5mm	Molex-SMA-73251-1290	Microstrip Line
 <p>1st and 2nd TRL Calibration Kits 1.5mm FR4 (40-S0-50-4.7pF(0805)) Verification of Dielectric in SMA 1.5mm RO4003C (40-S0-50-4.7pF(0805)) TUHH</p>			The 1st and 2nd calibration kits and the SMA model verified in the subsection 3.3
3rd	FR4 1.5mm	Molex-SMA-73251-1290	Microstrip Line
4th	FR4 1mm	Molex-SMA-73251-1290	Microstrip Line
 <p>3rd and 4th TRL Calibration Kits (Molex SMA 73251-1290) 1.5mm FR4 (40-S0-50-57-57-4.7pF(0805)) 1mm FR4 (40-S0-50-57-57-4.7pF(0805)) TUHH</p>			The 3rd and 4th calibration kits
5th	FR4 1mm	Rosenberger-SMA-32K243-40ML5	Microstrip Line
6th	FR4 1mm	Southwest-91Y60926	Microstrip Line
7th	FR4 1mm	Southwest-91Y60926	CPWG
 <p>5th, 6th and 7th TRL Calibration Kits 1mm-FR4-ML (40-S0-50-57-57-4.7pF(0805))-32K243-40ML5 1mm-FR4-ML (40-S0-50-52-(0402))-91Y60926 1mm-FR4-CPWG (40-S0-50-52-(0402))-91Y60926 TUHH</p>			The 5th, 6th and 7th calibration kits

There are totally seven calibration kits, the S-parameters of the kits are all shown in Fig. 80~Fig. 86.

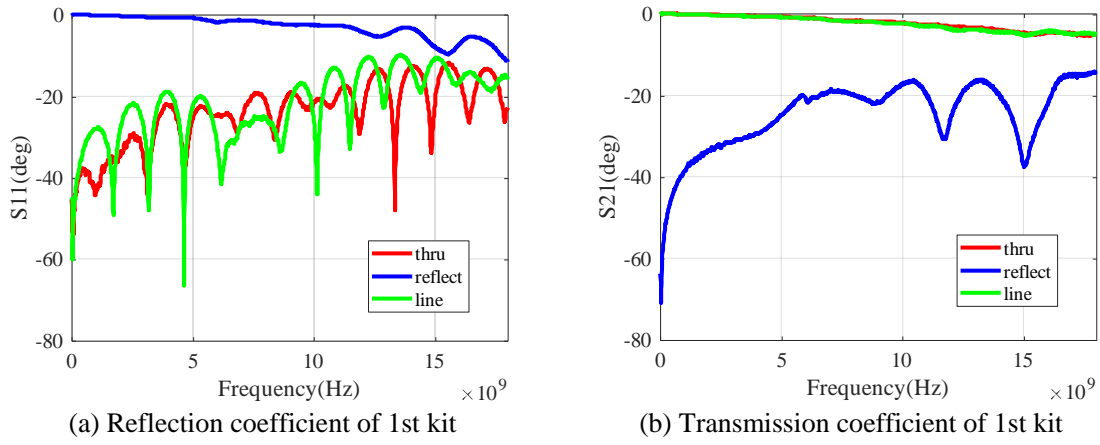


Fig. 80 S-parameter of the 1st calibration kit

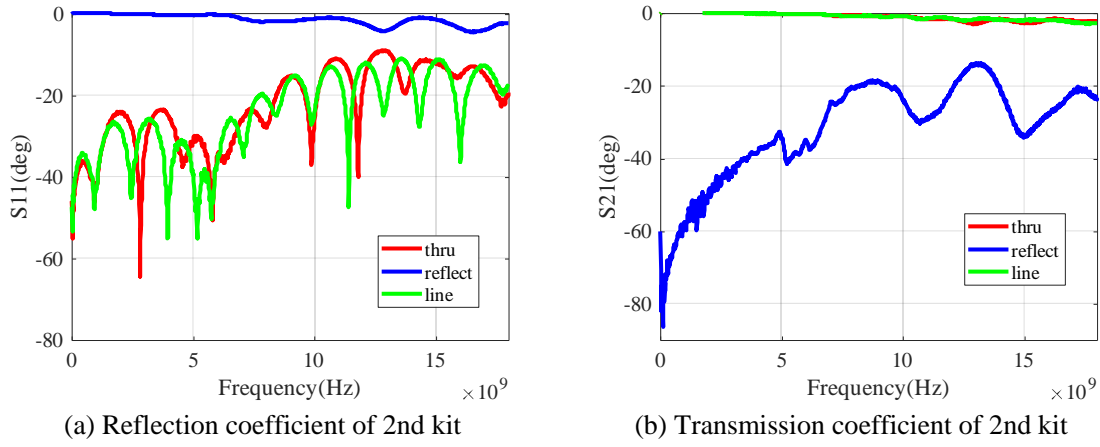


Fig. 81 S-parameter of the 2nd calibration kit

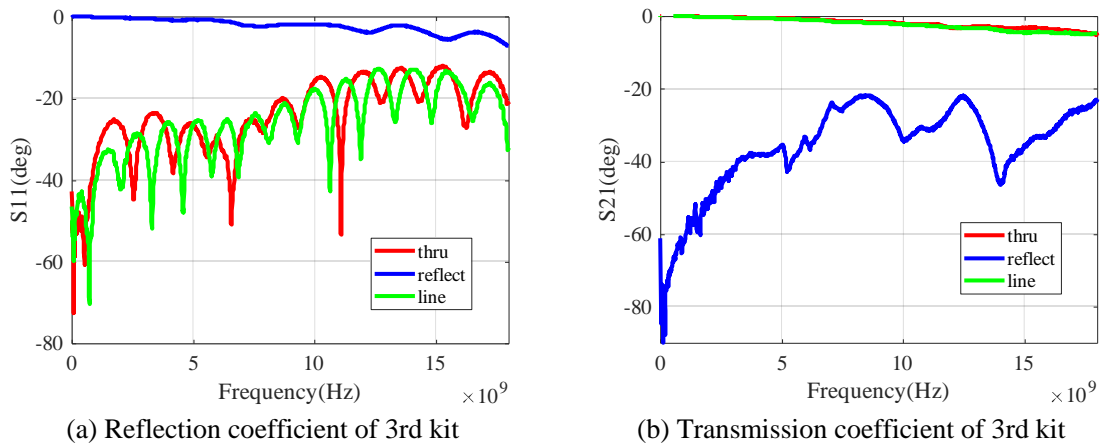
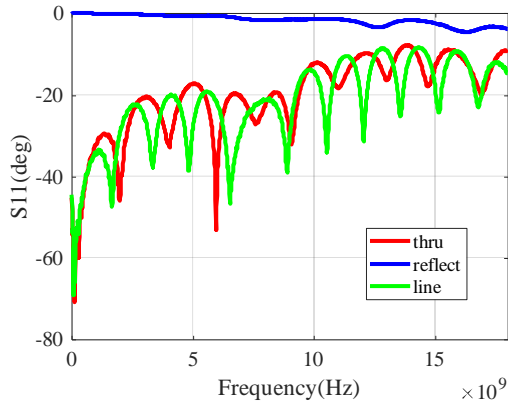
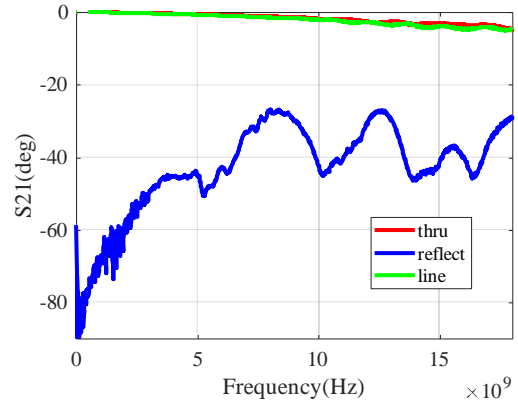


Fig. 82 S-parameter of the 3rd calibration kit

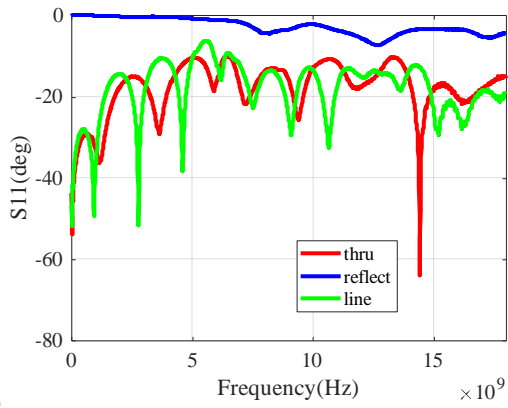


(a) Reflection coefficient of 4th kit

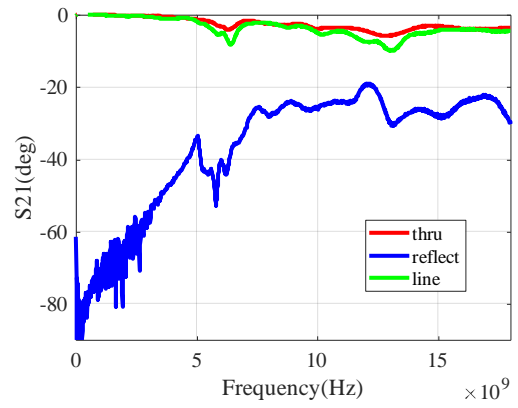


(b) Transmission coefficient of 4th kit

Fig. 83 S-parameter of the 4th calibration kit

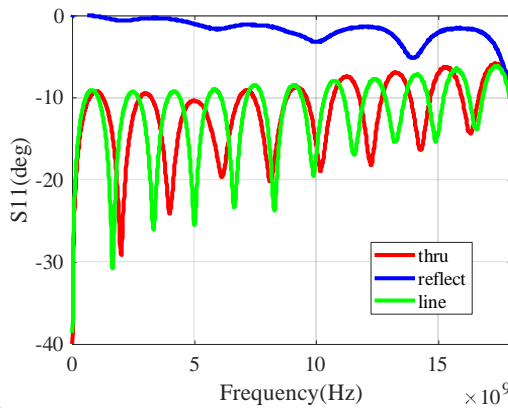


(a) Reflection coefficient of 5th kit

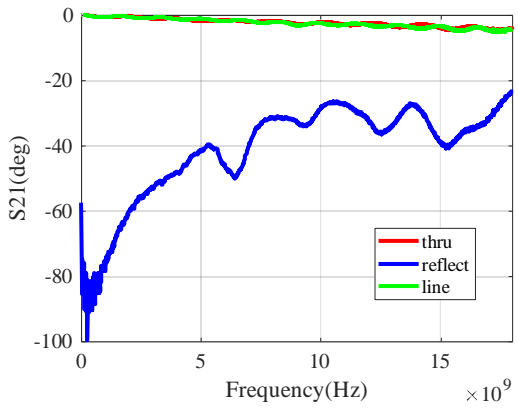


(b) Transmission coefficient of 5th kit

Fig. 84 S-parameter of the 5th calibration kit

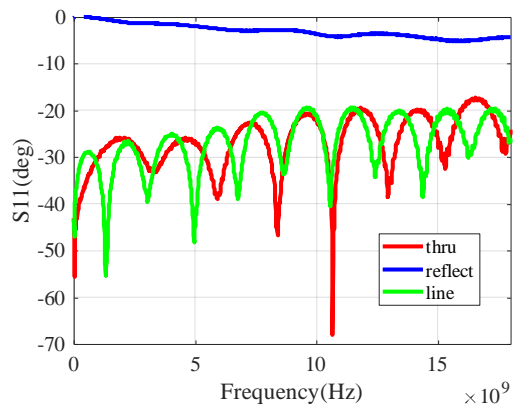


(a) Reflection coefficient of 6th kit

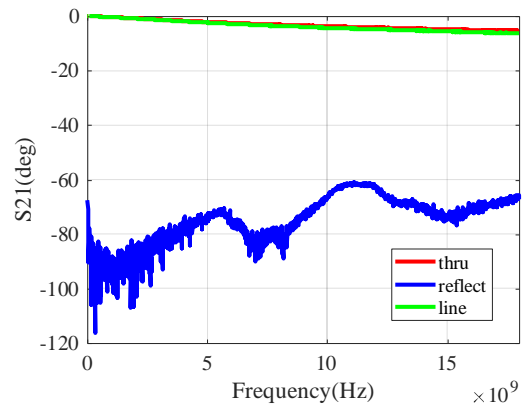


(b) Transmission coefficient of 6th kit

Fig. 85 S-parameter of the 6th calibration kit



(a) Reflection coefficient of 7th kit



(b) Transmission coefficient of 7th kit

Fig. 86 S-parameter of the 6th calibration kit

6. Conclusions and Recommendations

This research project supported by DAAD and CSC has been completed. The research content is sufficient and highly consistent with the original research plan, in some aspects, extended research has been done. The main research can be divided into three parts, summary and conclusion of this research project are drawn as follows.

(1) The first part of the project is the training of simulation and measurement. The scholarship holder intends to deepen the understanding of simulation calculations through modeling and simulation of research project models and similar models, improve efficiency for the coming two parts, meanwhile some inspiration for deepening or expanding projects are gained.

In the first part, FIT and FEM methods are both utilized in order to judge the credibility of the simulation results with the knowledge of electromagnetism. Comparison is analyzed for the judgment of whether the results are credible or not. Due to the difference in the algorithm principles of the two methods, sometimes the simulation results cannot be completely consistent, especially in multi-port simulation, but the results are acceptable. It depends on the 3D model, frequency range, the FEM method is more accurate when the 3D model is complex, and the FIT method is more accurate when implemented at high frequencies.

When some information of the model can be parameterized, sweep simulation can be implemented, not only to help observe the influence of parameters, but also to ensure the rationality of the simulation. Through sweeping, we can clearly observe the change of the result, which helps to judge whether the result is reliable, and also helps to optimize the simulation setting.

Programming is necessary in the calculation when calculation cannot be done by commercial software. But even if there is no error in the theoretical derivation, the calculation of the electromagnetic field is still complicated, involving the calculation of matrices, real numbers, and imaginary numbers. During the calculation process, phase changes are likely to cause errors in subsequent calculations, which must be carefully paid attention to.

(2) The second part of the project is the verification of the TRL calibration method, which is the de-embedding part of the original research plan. Compared with the previous part of work, the proportion of simulation work in this part is reduced, and the proportion of actual measurement job is greatly increased. In the measurement, we aim to match the test and the simulation, the dielectric permittivity of the SMA connector is adjusted through the verification of the phase.

In the high-frequency measurement up to 18GHz, the structure of the SMA connector is adjusted, and verified through simulation and experiment, the resonance formed by the fingers of the SMA connector is eliminated in the microstrip line. Often in industrial applications, due to production standards and mass production, products are reliable in most cases, but when used for research, the accuracy of product parameters and the effect of high-frequency applications cannot meet the requirements of performance breakthroughs, at this time moderate verification and adjustment are necessary.

(3) The third major part of the project is further de-embedding of the device, which is highly consistent with the model synthesis in the original research plan. In this part the feasibility of the further de-embedding method is verified through simulation, then the test data is substituted, the intrinsic parameters of element is calculated and brought into different application conditions, relatively consistent result is obtained. But in comparison, there is still a certain difference with the actual measurement result in the magnitude of S-parameters. This method is highly dependent on the consistency of simulation and measurement, so the job in the third part indirectly highlights the significance of the previous part. That is, the TRL standard eliminates the inconsistency between simulation and measurement that may be caused by coaxial to microstrip transition, which indicates that the forward and backward work of this research project is coherent and meaningful.

7 References

- [1] G. F. Engen, and C. A. Hoer. "Thru-reflect-line: An improved technique for calibrating the dual six-port automatic network analyzer." *IEEE Transactions on Microwave Theory and Techniques* vol. 27, no. 12, pp. 987-993, 1979.
- [2] L. F. Chen, C. K. Ong, C. P. Neo, V. V. Varadan, and V. K. Varadan, *Microwave electronics: measurement and materials characterization*, John Wiley & Sons, 2004.
- [3] B. Gustavsen, and A. Semlyen, "Rational Approximation of Frequency Domain Responses by Vector Fitting," *IEEE Transactions on Power Delivery*, vol. 14, no. 3, pp. 1052-1061, 1999.
- [4] S. Grivet-Talocia. "Passivity Enforcement via Perturbation of Hamiltonian Matrices." *IEEE Transactions on Circuits and Systems I: Regular Papers*, vol. 51, no. 9, (2004): 1755-1769.
- [5] V. I. Okhmatovski, J. Morsey, and A. C. Cangellaris. "On Deembedding of Port Discontinuities in Full-wave CAD Models of Multiport Circuits," *IEEE Transactions on Microwave Theory and Techniques*, vol. 51, no. 12, (2003): 2355-2365.
- [6] M. Yousefbei, and J. Perruisseau-Carrier. "A Practical Technique for Accurately Modeling Reconfigurable Lumped Components in Commercial Full-wave Solvers," *IEEE Antennas and Propagation Magazine*, vol. 54, no. 5 (2012): 298-303.
- [7] W.-Z. Wang, R. Jin, T. S. Bird, X. Liang and J. Geng. "De-embedding based on EM simulation and measurement: A hybrid method." *IEEE Transactions on Microwave Theory and Techniques*, vol. 65, no. 12, (2017): 5019-5034.
- [8] G. Jian, Zh.-H. Zhang, and C. Qian, "Modeling of commercial millimeter wave Schottky diodes." *2016 IEEE International Conference on Microwave and Millimeter Wave Technology (ICMMT)*. Vol. 1. IEEE, 2016.
- [9] B. Isabella, S. Skidmore, and L. Dunleavy, "3D surface mount component modeling for HFSS." *2018 IEEE 19th Wireless and Microwave Technology Conference (WAMICON)*. IEEE, 2018.
- [10] Y. F. Qian, Z. F. Ye, and H. B. Zhang, "Impact of Modeling Simplifications on Lightning Strike Simulation for Aeroengine". *Mathematical Problems in Engineering*, vol. 2019, Article ID 5176560, 11 pages, 2019.
- [11] C. Yang, H. D. Brüns, P. G. Liu, and C. Schuster, "Impulse response optimization of band-limited frequency data for hybrid field-circuit simulation of large-scale energy-selective diode grids." *IEEE Transactions on Electromagnetic Compatibility*, vol. 58, no. 4, 2016, pp. 1072-1080.
- [12] CONCEPT-II. Institut für Theoretische Elektrotechnik. Hamburg, Germany. [Online]. Available: www.tet.tuhh.de/concept
- [13] Dennis M. Sullivan, *Electromagnetic Simulation using the FDTD Method*, IEEE press series on RF and Microwave Technology, 2000.
- [14] CST Studio Suite® 2020 Help, https://space.mit.edu/RADIO/CST_online/cst_studio_suite_help.htm.
- [15] HFSS™ Online Help, http://www.ece.uprm.edu/~rafaelr/inel6068/HFSS/hfss_onlinehelp.pdf
- [16] Henry W. Ott. "Electromagnetic Compatibility Engineering," John Wiley & Sons, 2009.
- [17] <https://www.3ds.com/products-services/simulia/resources/microstrip-transmission-line/>
- [18] Michael D. Janezic and Jeffrey A. Jargon, "Complex Permittivity Determination from Propagation Constant Measurements," *IEEE Microwave and Guided Wave Letters*, vol. 9, no. 2, February 1999.
- [19] <https://qas-ecatalog.hubersuhner.com/media/documents/datasheet/en/pdf/84003373>.
- [20] <https://qas-ecatalog.hubersuhner.com/media/documents/datasheet/en/pdf/84004007>.
- [21] <https://qas-ecatalog.hubersuhner.com/media/documents/datasheet/en/pdf/84002061>.
- [22] IEEE Standard for Electrical Characterization of Printed Circuit Board and Related Interconnects at Frequencies up to 50 GHz, IEEE Standard 370-2020, 2021
- [23] C. Seguinot, P. Kennis, J. Legier, F. Huret, E. Paleczny, and L. Hayden, "Multimode TRL—A New Concept in Microwave Measurements: Theory and Experimental Verification," *IEEE Transactions on Microwave Theory and Techniques*, vol. 46, no. 5, pp. 536-542, May 1998.
- [24] https://www.distrelec.de/Web/Downloads/_d/wg/73251-1290_eng_dwg.pdf.
- [25] Z. -N. Ariga, K. Wada and T. Shimizu, "TDR Measurement Method for Voltage-Dependent Capacitance of Power Devices and Components," *IEEE Transactions on Power Electronics*, vol. 27, no. 7, pp. 3444-3451.

- [26] G. Jian, Zh.-H. Zhang, and C. Qian. "Modeling of commercial millimeter wave Schottky diodes." 2016 IEEE International Conference on Microwave and Millimeter Wave Technology (ICMMT). Vol. 1. IEEE, 2016.
- [27] B. Isabella, S. Skidmore, and L. Dunleavy. "3D surface mount component modeling for HFSS," 2018 IEEE 19th Wireless and Microwave Technology Conference (WAMICON). IEEE, 2018.
- [28] P. Li, C. Chou and T. Wu, "Modeling of Radiated Emission caused by Coaxial-to-microstrip Transition," 2019 International Conference on Electromagnetics in Advanced Applications (ICEAA), 2019, pp. 245-249.
- [29] Krishna K. Agarwal and Richard R. Harlan, "Coax-to-microstrip transition," U.S. Patent, 5418505, May 23, 1995.
- [30] E. S. Li, H. Wu and H. Huang, "Solving Resonance Problems in Transitions: End-Launch Connector Considerations for Coaxial-to-Microstrip Transitions," IEEE Microwave Magazine, vol. 20, no. 3, pp. 64-75, March 2019.
- [31] E. H. England, "A Coaxial to Microstrip Transition (Short Papers)," IEEE Transactions on Microwave Theory and Techniques, vol. 24, no. 1, pp. 47-48, Jan. 1976.
- [32] E. S. Li, J. C. Cheng and W. Y. Tai, "Extending the Operation Frequencies of Standard Coaxial-to-Microstrip Connectors," Microwave and Optical Technology Letters, vol. 01, no. 01, pp. 2716-2719, Dec. 2012.
- [33] J. C. Cheng, E. S. Li, W. F. Chou, "Improving the High-Frequency Performance of Coaxial-to-Microstrip Transitions," IEEE Transactions on Microwave Theory and Techniques, vol. 59, no. 6, pp. 1468-1477, Jun. 2011.
- [34] T. T. Ha. Solid-State Microwave Amplifier Design. USA: Wiley-Interscience, 1981, pp. 16.
- [35] X. Wang, W. Wang, Y. Liang and R. Jin, "1-Thru Deembedding Method for One-Port Microwave Device Characterization," in IEEE Microwave and Wireless Components Letters, vol. 32, no. 4, pp. 355-358, April 2022.
- [36] R. Wang, C. Li and Y. Wang, "An Improved Through-Only De-Embedding Method for 110-GHz On-Wafer RF Device Characterization," in IEEE Microwave and Wireless Components Letters, vol. 32, no. 10, pp. 1219-1222, Oct. 2022.
- [37] S. Yao, X. -C. Wei and L. Ding, "A Deembedding Method for the S-Parameter Extraction of Surface-Mounted Devices With Asymmetric Fixtures," in IEEE Microwave and Wireless Components Letters, vol. 31, no. 2, pp. 211-214.